University of Bucharest

Department of Chemical Technology and Catalysis

Nanostructuri catalitice continand metale nobile: sinteza, caracterizare si comportare catalitica

Vasile I. Pârvulescu

Diaspora în cercetarea ştiinţifică şi învăţământul superior din România, Bucureşti, 21-24 septembrie 2010

Workshop Exploratoriu: "Nano Sisteme Dinamice: de la Concepte la Aplicatii Senzoristice"

Size dependent properties of nanoparticles

- magnetic
- optical
- melting points
- specific heats
- surface reactivity
- **CATALYTIC**

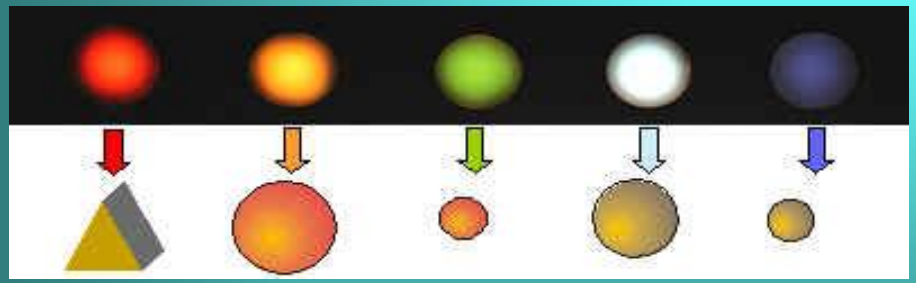

Ag(12nm) Au(100nm) Au(50nm) Ag(90nm) Ag(40nm)

Colors of light scattered by solutions of nanoparticles of certain sizes

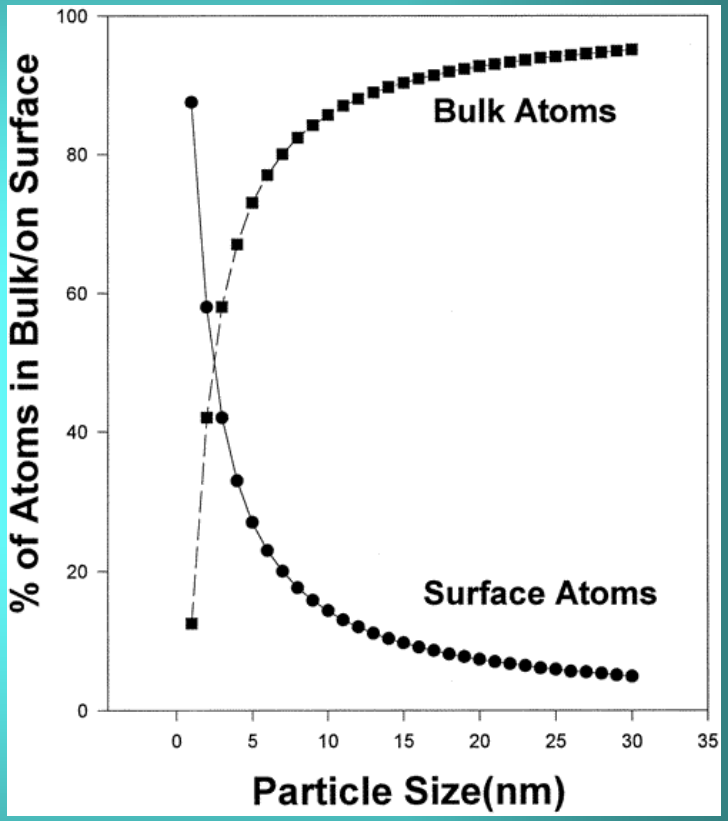

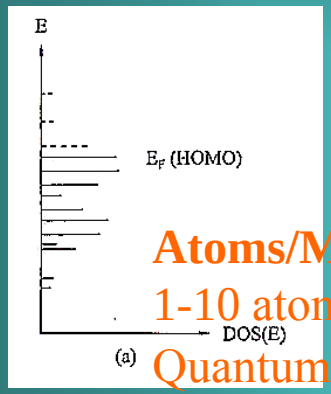

Atoms/Molecules
1-10 atoms
Quantum Chemistry

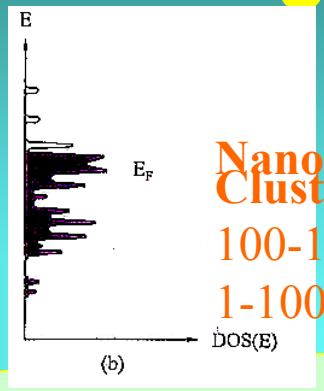

Nanoscale Clusters/Particles
100-100,000 atoms
1-100 nm in diameter

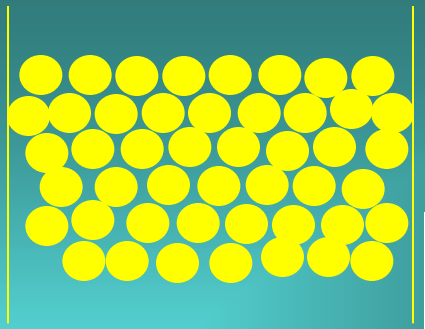

Condensed Matter
Millions of atoms
Solid State Physics

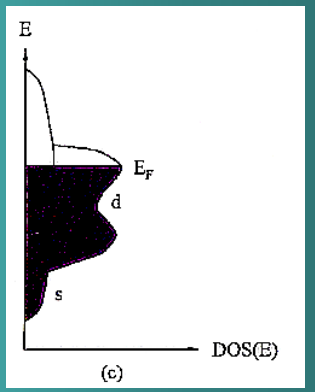

Novel Preparations

Catalysis

C-C coupling

Aerobic oxidations

Fuel cells

Heterogeneous enantioselective

Hydrogenations

Size dependent properties of nano

supported nano-structures

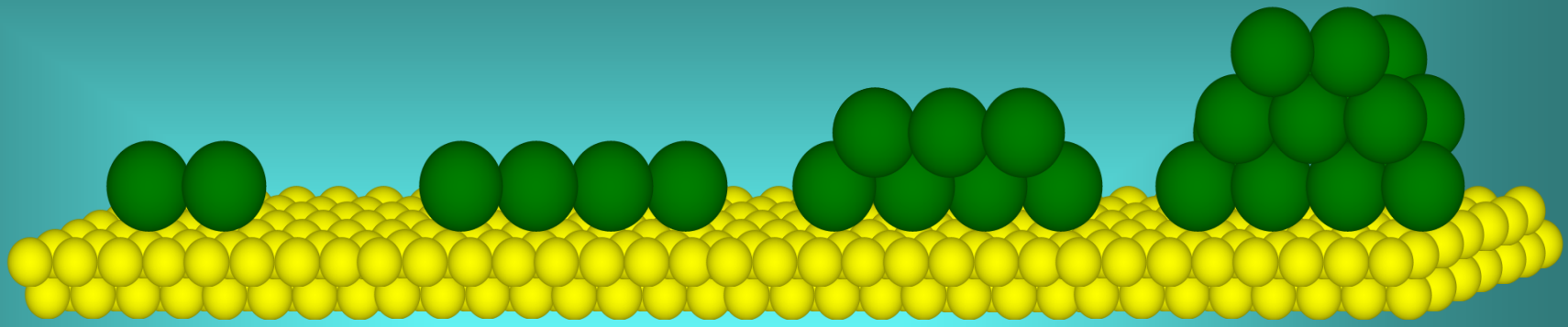

structural embedded nano-structures

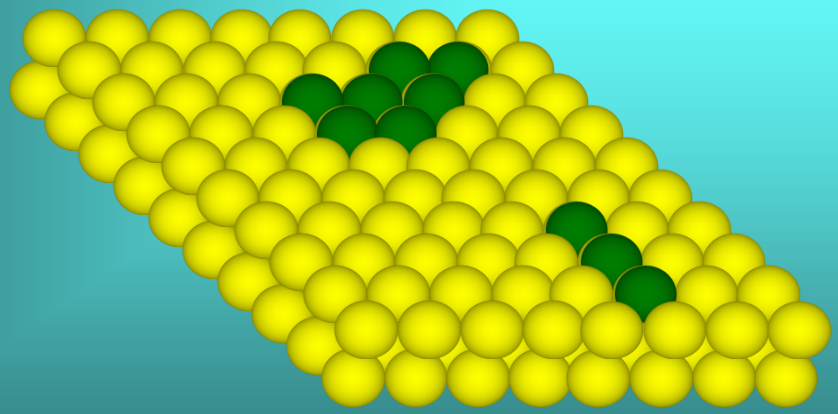

textural embedded nano-structures

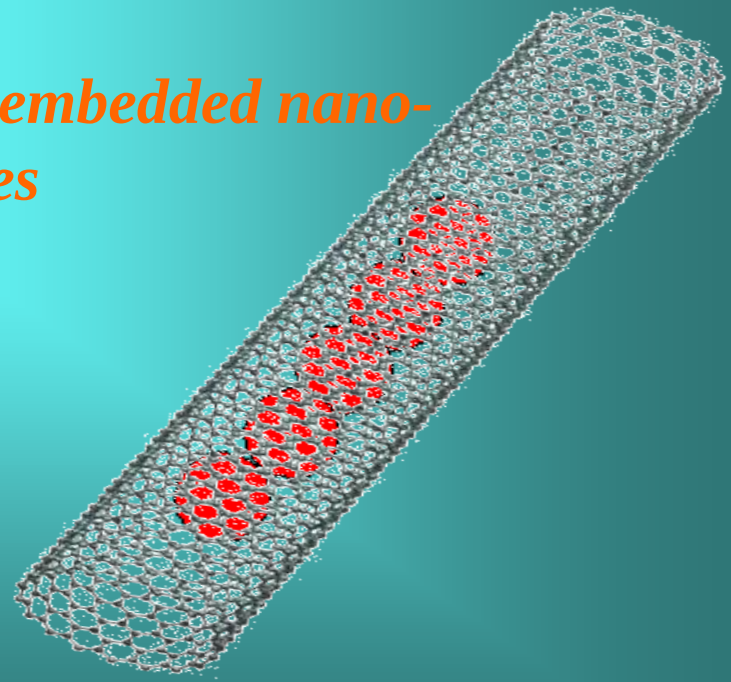

Size controlled Nanoparticles in Heterogeneous catalysis

Heterogeneous catalysts generally consist of a high surface area support material onto which an active component has been deposited. The anchoring of active component onto the support can be carried out via a number of methods such as homogeneous deposition precipitation, ion-exchange, chemical vapor deposition and (incipient) wetness impregnation. From an industrial point of view the latter type of technique is most often favored because of its technical simplicity, low amount of waste streams and low costs. This method is based on the incorporation of active component via impregnation of a solution containing a precursor, which is typically a metal salt. By applying thermal treatments the precursor is deposited onto the support and subsequently converted into the catalytic active species.

The chemistry involved in impregnation is very complicated since many processes take place during the impregnation, drying and activation steps. It is a well-known fact that the properties of the precursor solution (e.g. type of metal salt and pH) and support (e.g. texture and surface reactivity) largely affect the final composition of the catalyst. However, still little is known about the separate influences of precursor and support on the impregnation, drying and activation processes.

Size controlled Nanoparticles in Heterogeneous catalysis

Ionic exchange

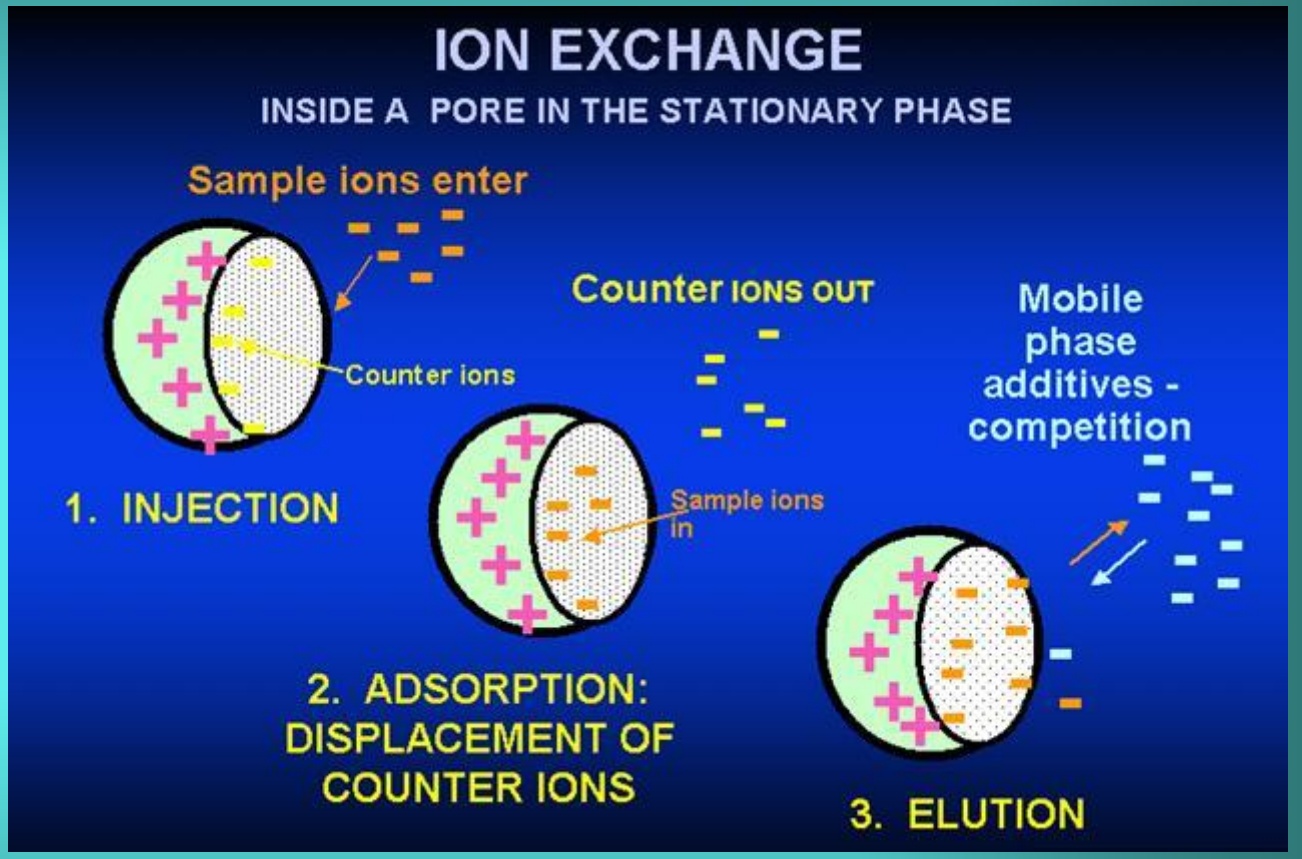

Materials: acidic (zeolites, clays), basic (LDH)

Size controlled Nanoparticles in Heterogeneous catalysis

Deposition-precipitation

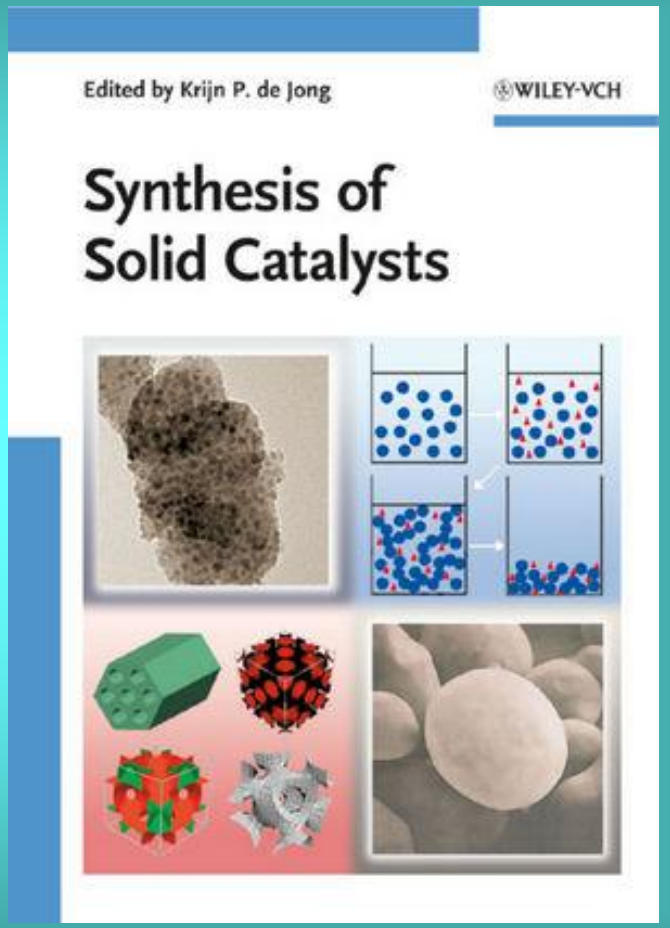

Materials: a very large variety including nano- and bulk materials, porous and non-porous supports

Ionic exchange: low metal loading iridium catalysts

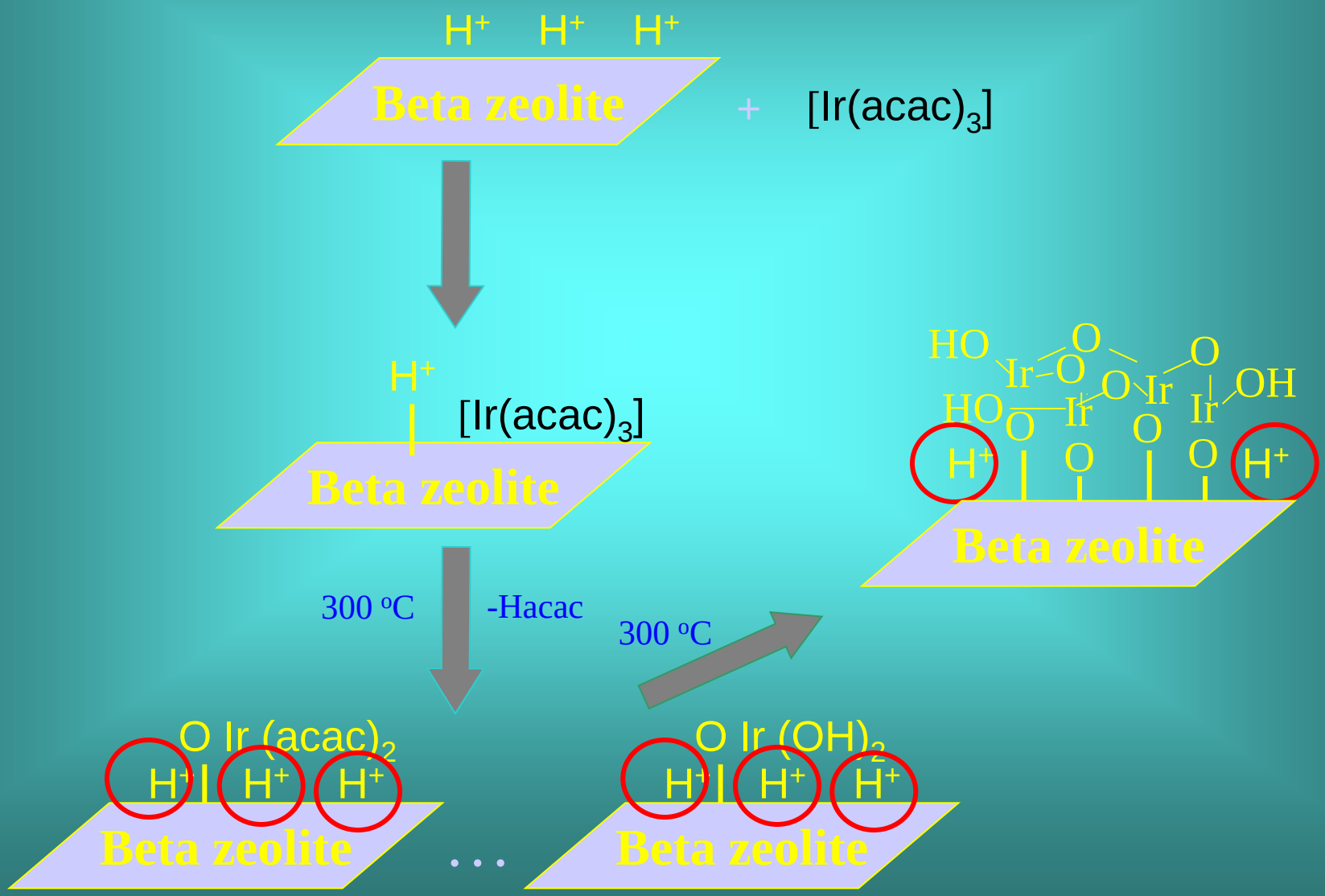

Catalysts preparation

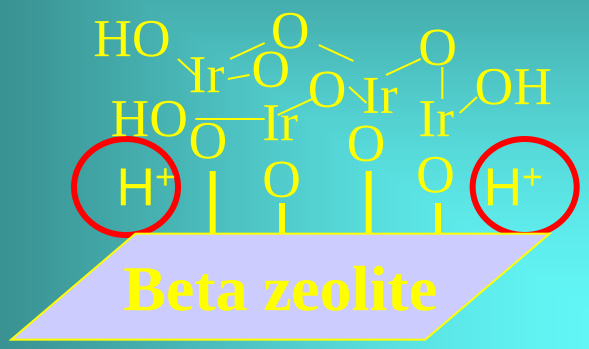

1.0% Ir/BEA
2.0% Ir/BEA
3.0% Ir/BEA
5.0% Ir/BEA

flowing H_2 at
250 or 450°C

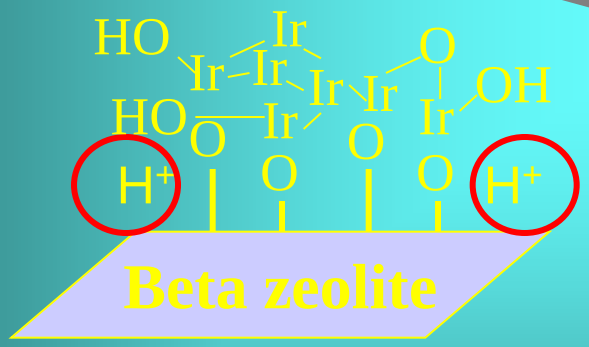

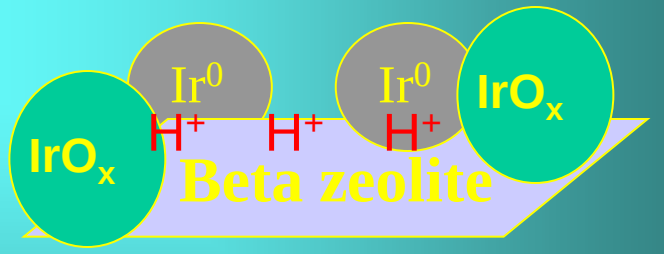

The deposition of iridium on BETA zeolite involves succesive ion-exchange and condensation processes. The generation of new protons is also possible.

Catalytic reaction: synthesis of prostaglandin derivatives

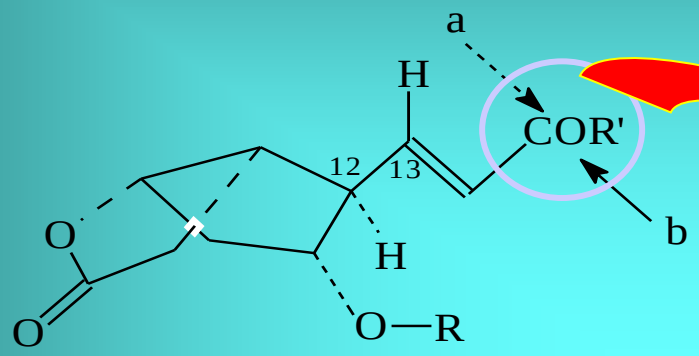

R = H, CH_3, C_2H_5, C_3H_7
R' = $OC_6H_4(mCl)$

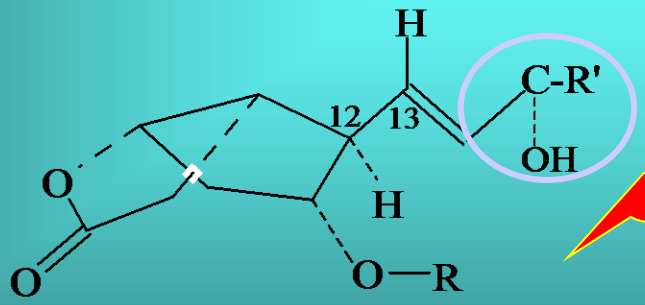

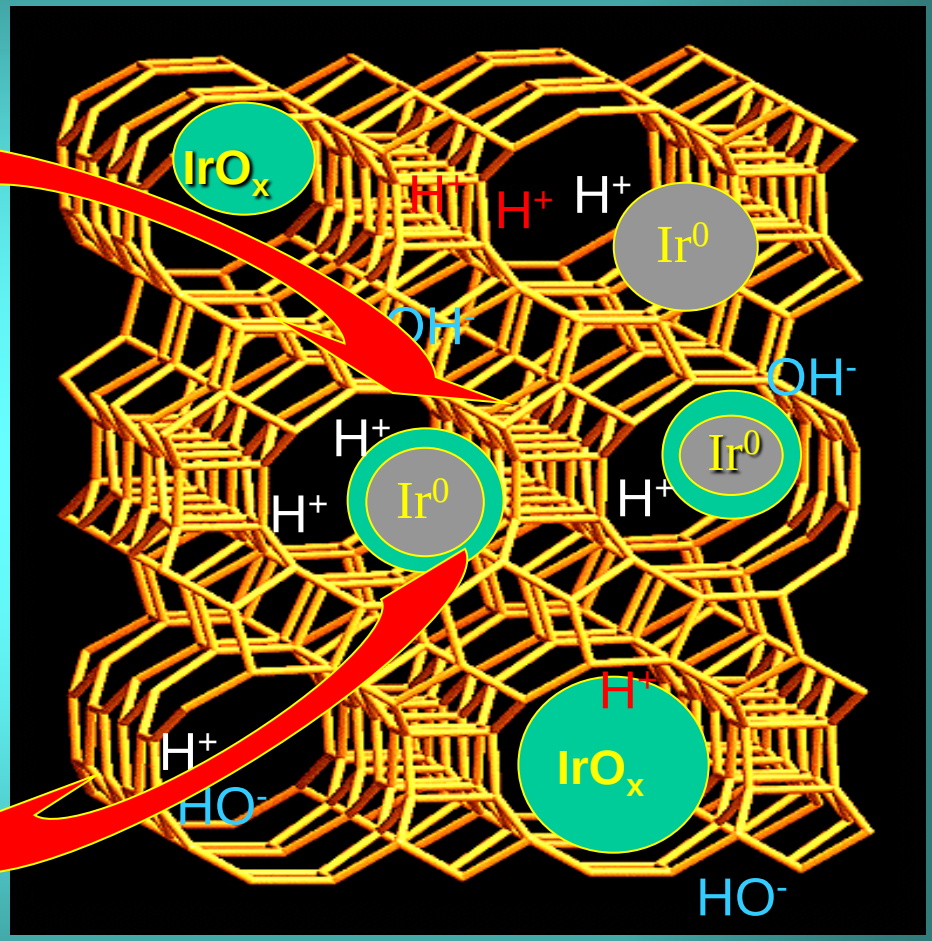

Angew. Chem., Int. Ed. Engl., 115 (2003) 5491-5494.

Hydrogenation of enones

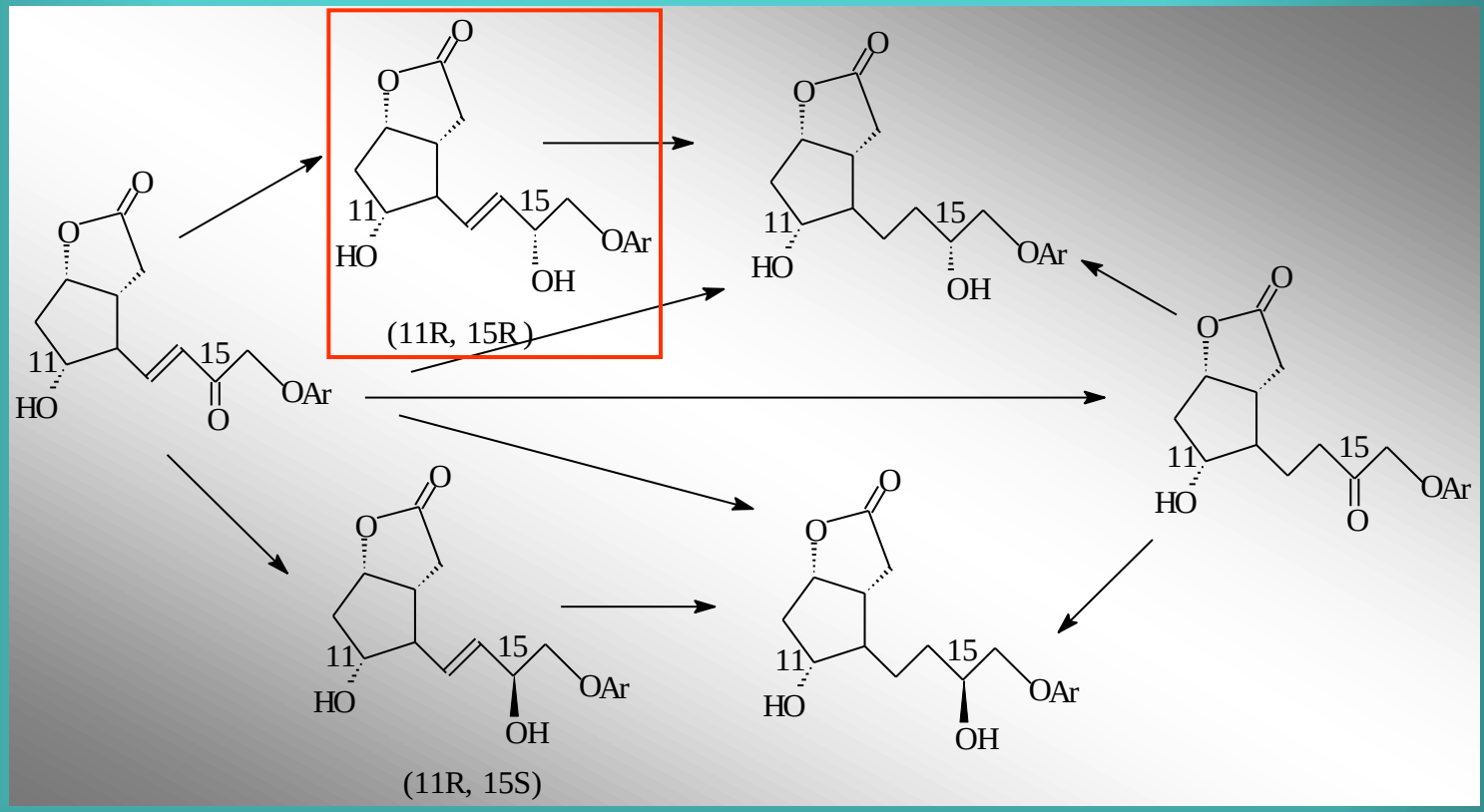

Optimal catalyst

450ºC

Temperature re

BEA zeolite

the support

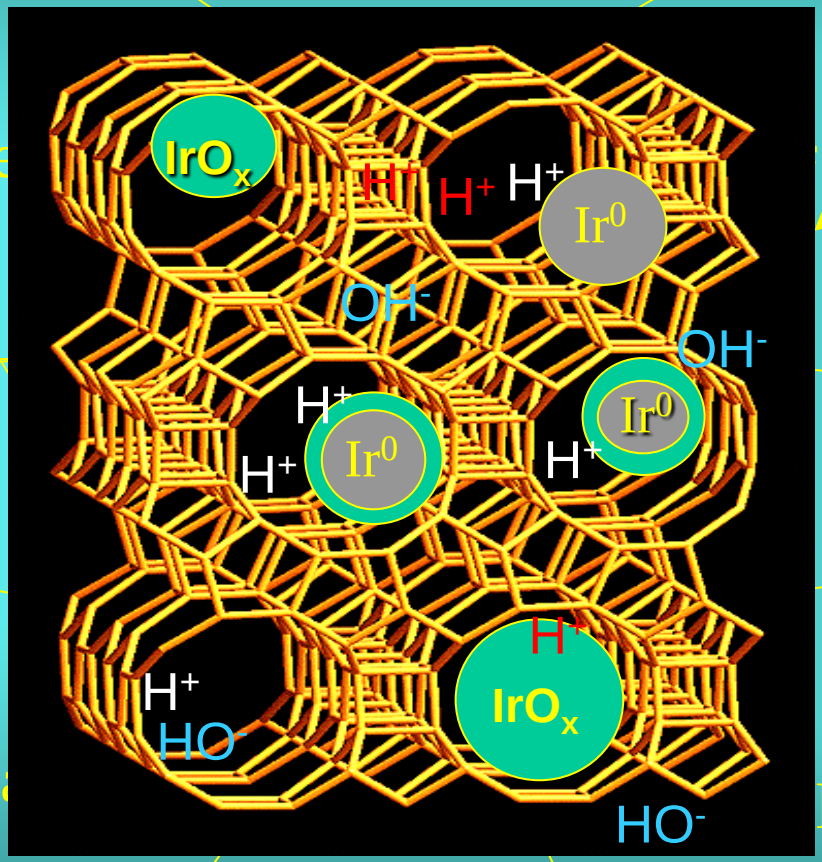

Support calcina

loading, %wt

NON PRECALCINED

1% Ir

Angew. Chem., Int. Ed. Engl., 115 (2003) 5491-5494.

Why 1% Ir/beta????????

Reduction degree, hydrogen up-take and Ir dispersion on beta-zeolites

Catalyst	Reduction temperature					
	250 °C			**450 °C**		
	Reduction degree, %	H_2 up-take, $cm^3\ g^{-1}$	Metal dispersion, %	Reduction degree, %	H_2 up-take, $cm^3\ g^{-1}$	Metal dispersion, %
1%Ir/BEA	14	0.03	**18.2**	**25**	0.05	**17.1**
2%Ir/BEA	27	0.05	8.6	38	0.07	8.1
3%Ir/BEA	58	0.08	3.9	67	0.08	3.4
5%Ir/Beta	69	0.12	3.1	81	0.11	2.4
1%Ir/Beta-5	14	0.03	19.2	24	0.05	18.3
2%Ir/Beta-5	24	0.05	9.6	36	0.08	9.2
3%Ir/BEA-500	54	0.10	5.5	66	0.11	4.9
5%Ir/Beta-5	67	0.18	4.7	77	0.18	4.1
1%Ir/Beta-7	13	0.03	19.5	21	0.05	19.8
2%Ir/Beta-7	23	0.06	11.7	35	0.09	10.8
3%Ir/Beta-7	50	0.13	7.5	62	0.14	6.5
5%Ir/Beta-7	63	0.25	6.8	73	0.26	6.0

Reduction degree, hydrogen up-take and Ir dispersion on beta-zeolites

Catalyst	Reduction degree, %	H_2 up-take, $cm^3\ g^{-1}$	Metal dispersion, %
1%Ir/MCM-41	36	0.14	33.4
2%Ir/MCM-41	48	0.16	14.6
3%Ir/MCM-41	75	0.25	9.4
5%Ir/MCM-41	89	0.34	6.5
1%Ir/SiO_2	37	0.04	9.4
2%Ir/SiO_2	46	0.05	4.3
3%Ir/SiO_2	77	0.07	2.6
5%Ir/SiO_2	88	0.09	1.7
1%Ir/ZrO_2	29	0.02	6.8
2%Ir/ZrO_2	44	0.04	3.8
3%Ir/ZrO_2	71	0.05	2.2
5%Ir/ZrO_2	85	0.07	1.4

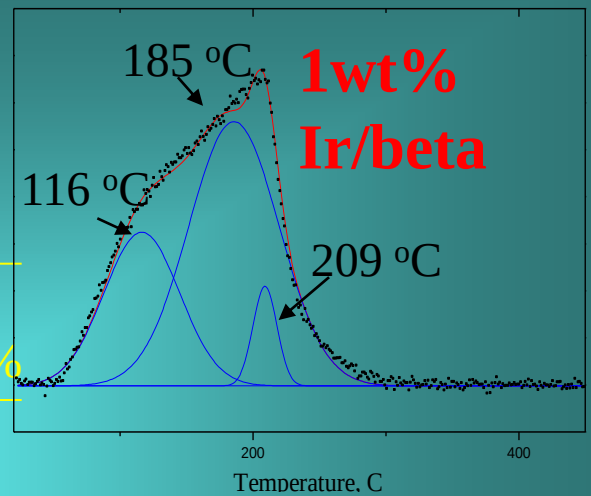

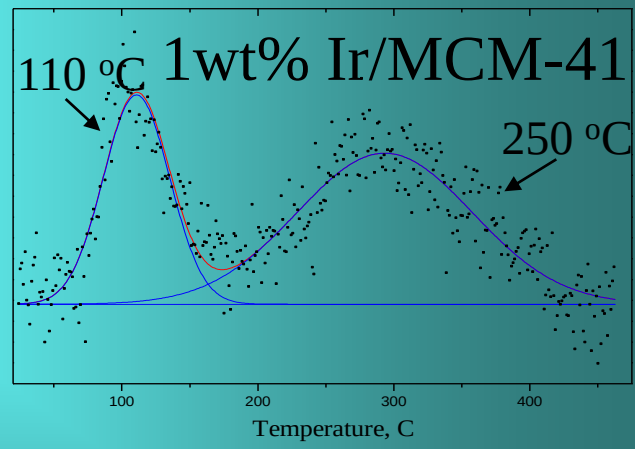

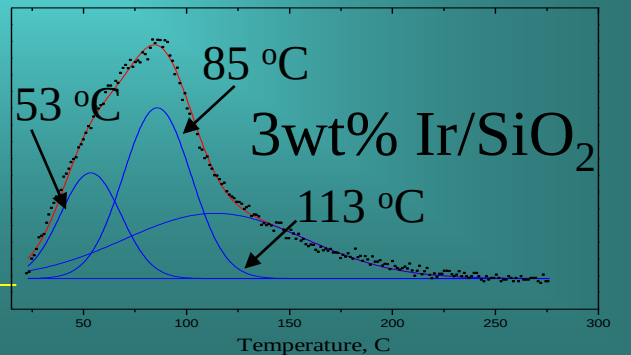

XPS Binding energies, and Ir^o/Ir^{n+} and Ir/Si(Zr) ratios

Catalyst	Binding energy of Ir levels, eV				Ir^o/Ir^{n+} ratio	Binding energy, eV			Comparative Ir/Si ratios x 10^3	
	Ir^0		Ir^{n+}							
	$Ir_{4f7/2}$	$Ir_{4f5/2}$	$Ir_{4f7/2}$	$Ir_{4f5/2}$		Si_{2p}	Al_{2p}	O_{1s}	Analytic	XPS
1%Ir/BEA	61.4	64.6	63.2	65.4	**0.42**	103.5	74.8	532.8	**3.3**	**6.0**
1%Ir/BEA**	61.5	64.7	63.3	65.5	**0.38**	103.5	74.8	532.8	**3.3**	**6.2**
1%Ir/BEA***	61.5	64.7	63.3	65.5	**0.31**	103.5	74.8	532.8	**3.3**	**5.9**
2%Ir/BEA	61.2	64.4	63.0	65.0	**1.02**	103.6	74.8	532.8	**6.6**	**11.2**
3%Ir/BEA	61.2	64.2	62.7	65.1	**1.70**	103.6	74.6	532.8	**9.9**	**20.6**
5%Ir/BEA	61.2	64.3	62.6	65.2	**1.47**	103.6	74.7	532.8	**16.5**	**42.1**
1%Ir/MCM-41	61.2	64.4	62.5	65.0	**1.71**	103.8	-	533.0	**3.1**	**2.5**
1%Ir/SiO_2	61.5	64.6	62.5	65.3	**1.68**	103.7	-	532.8	**9.6**	**20.0**
1%Ir/ZrO_2*	61.7	64.8	62.3	65.2	**0.31**	-*	-	531.9	**6.4** Zr: **16.7**	**40.0**

*-The binding energy of Zr_{3d}: 182.2 eV; **-zeolite precalcined at 700 °C; ***- catalyst reduced at 250 °C.

^{193}Ir Mossbauer spectrum

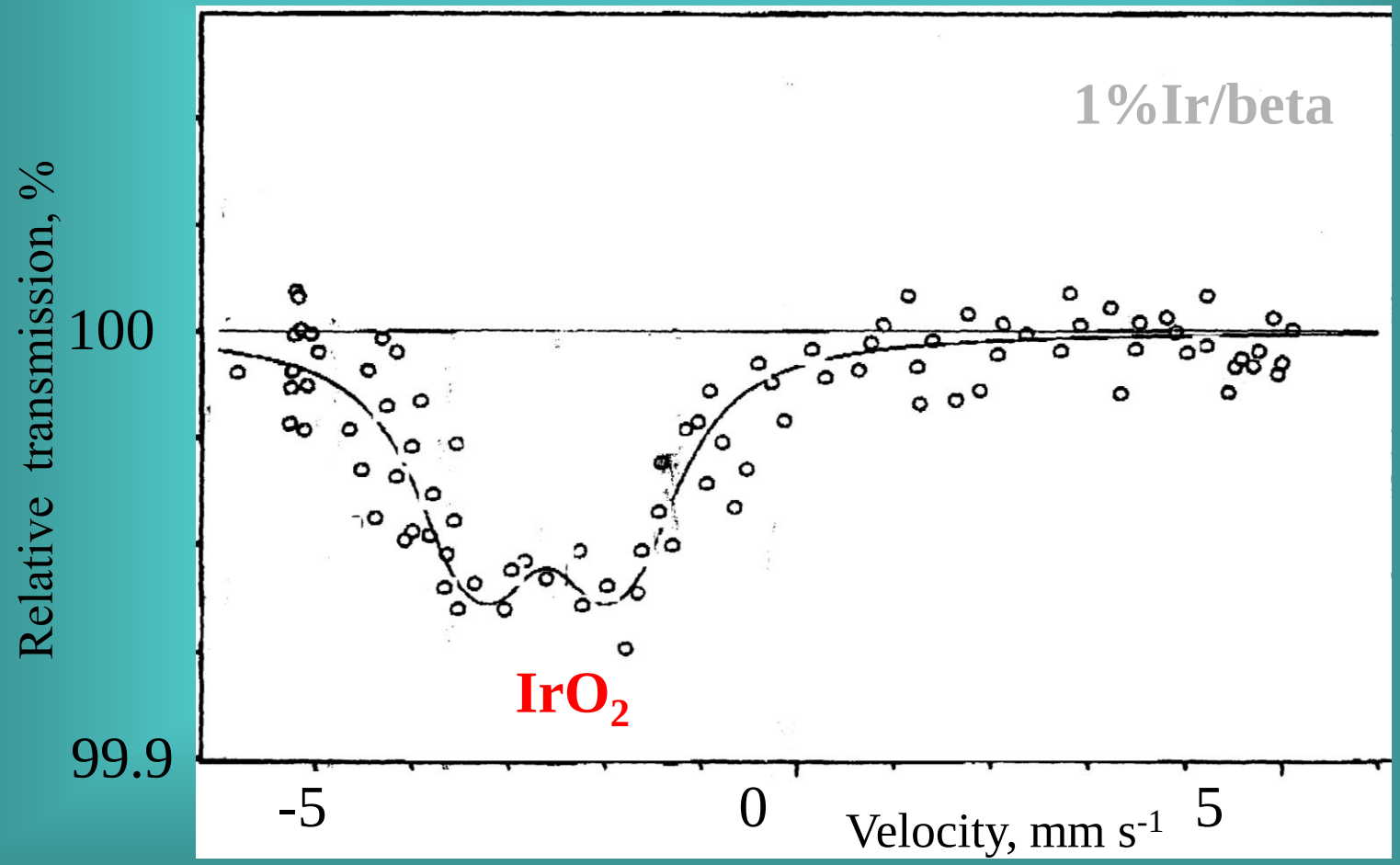

Py-FT-IR

Desorption temperature: 200 ºC

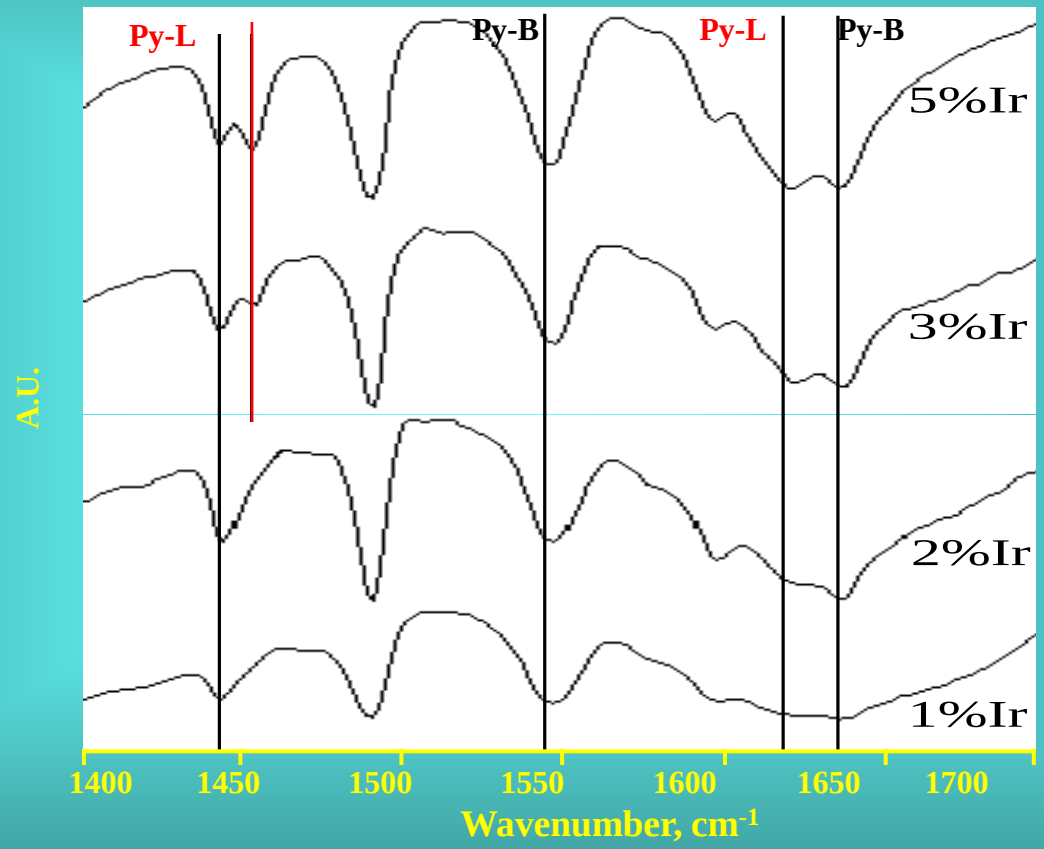

The new band at 1453 cm^{-1} may suggest either the existence of a new Lewis site (Ir^{n+}) or the re-adsorption of Py via H bonds forming Py-H species (also assigned to the presence of Ir).

CP/MAS ^{27}Al-NMR

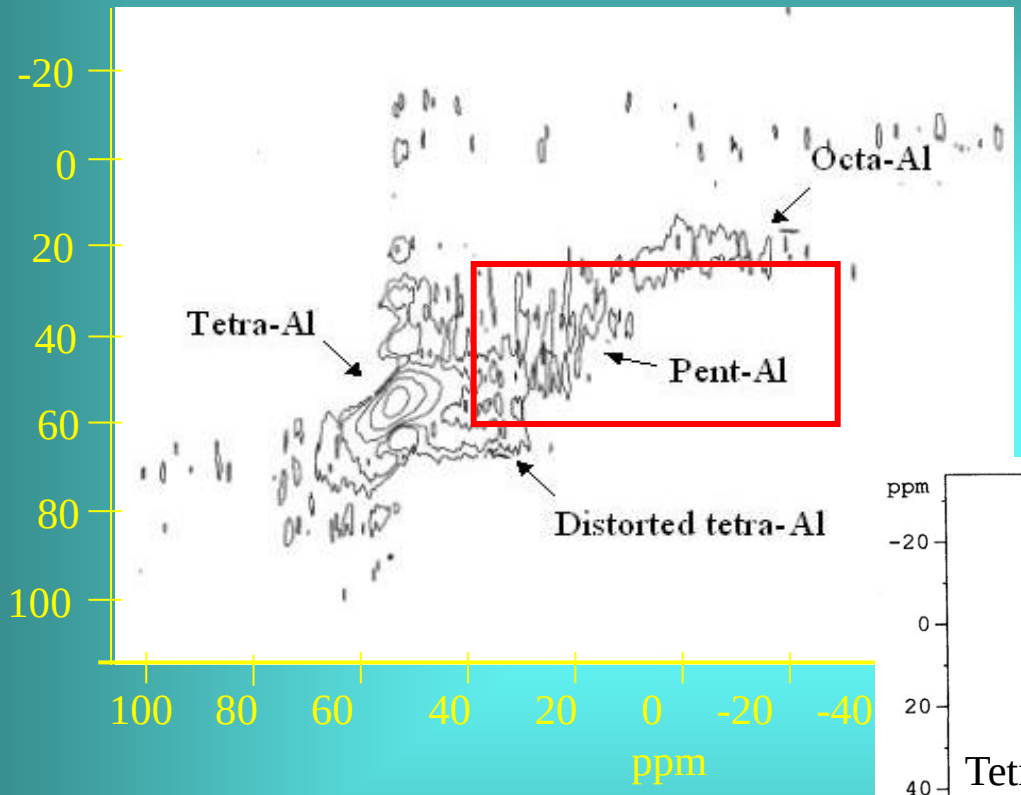

BEA zeolite calcined at 700^{0}C

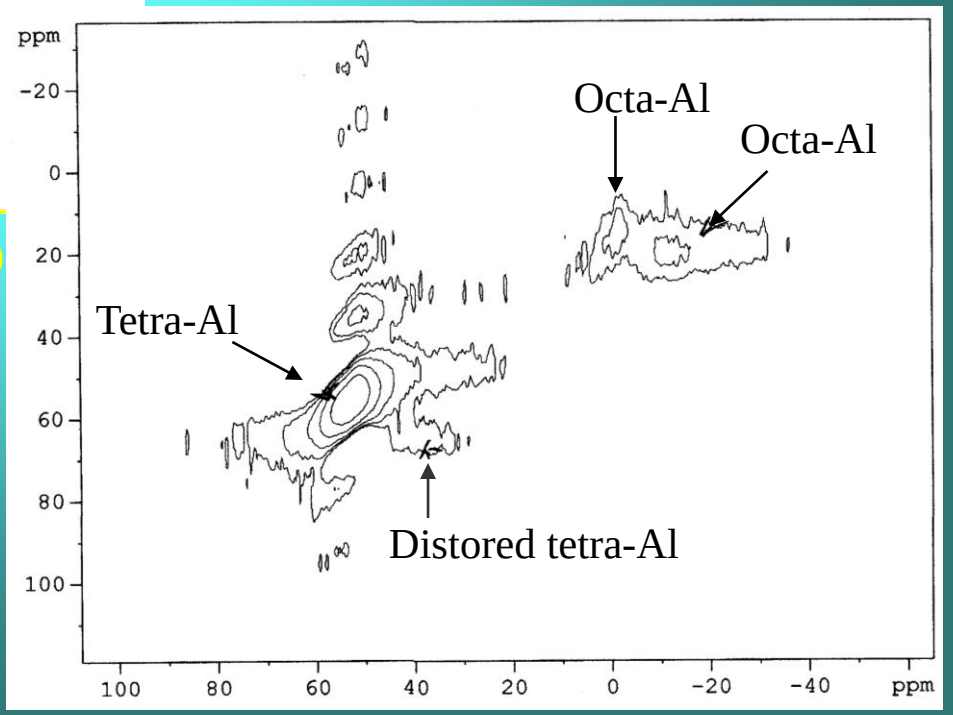

BEA zeolite uncalcined

Reaction mechanism

Cram-chelate rule

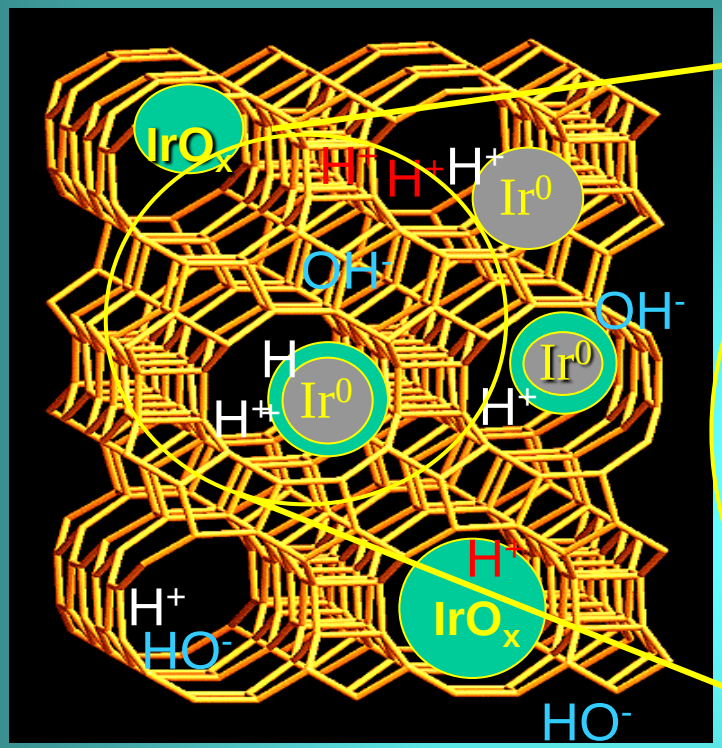

Lewis acid centers:

Al^{3+} (Ir^{3+}) + H_2 ⟶ $H^+ + H^-$

Metallic centers:

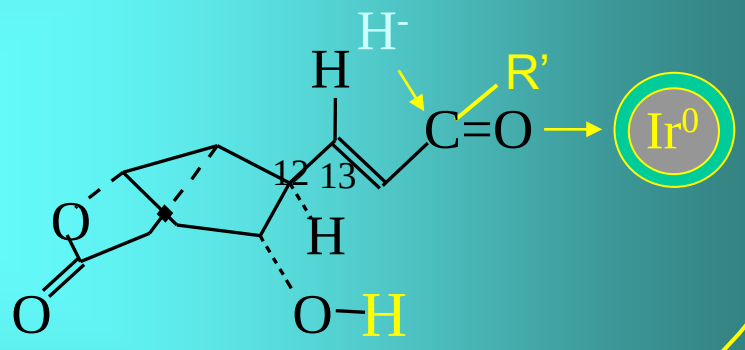

R' = $OC_6H_4(mCl)$

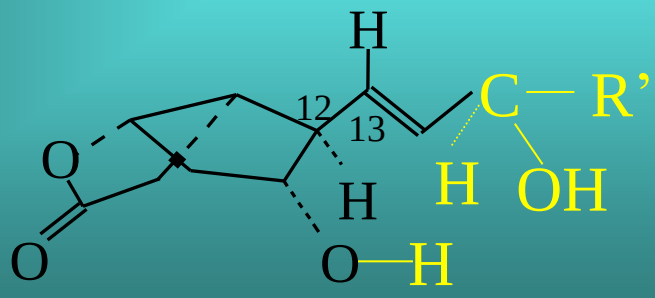

Angew. Chem., Int. Ed. Engl., 115 (2003) 5491-5494.

Effect of the particle size:

Synthesis of menthols from citronellal

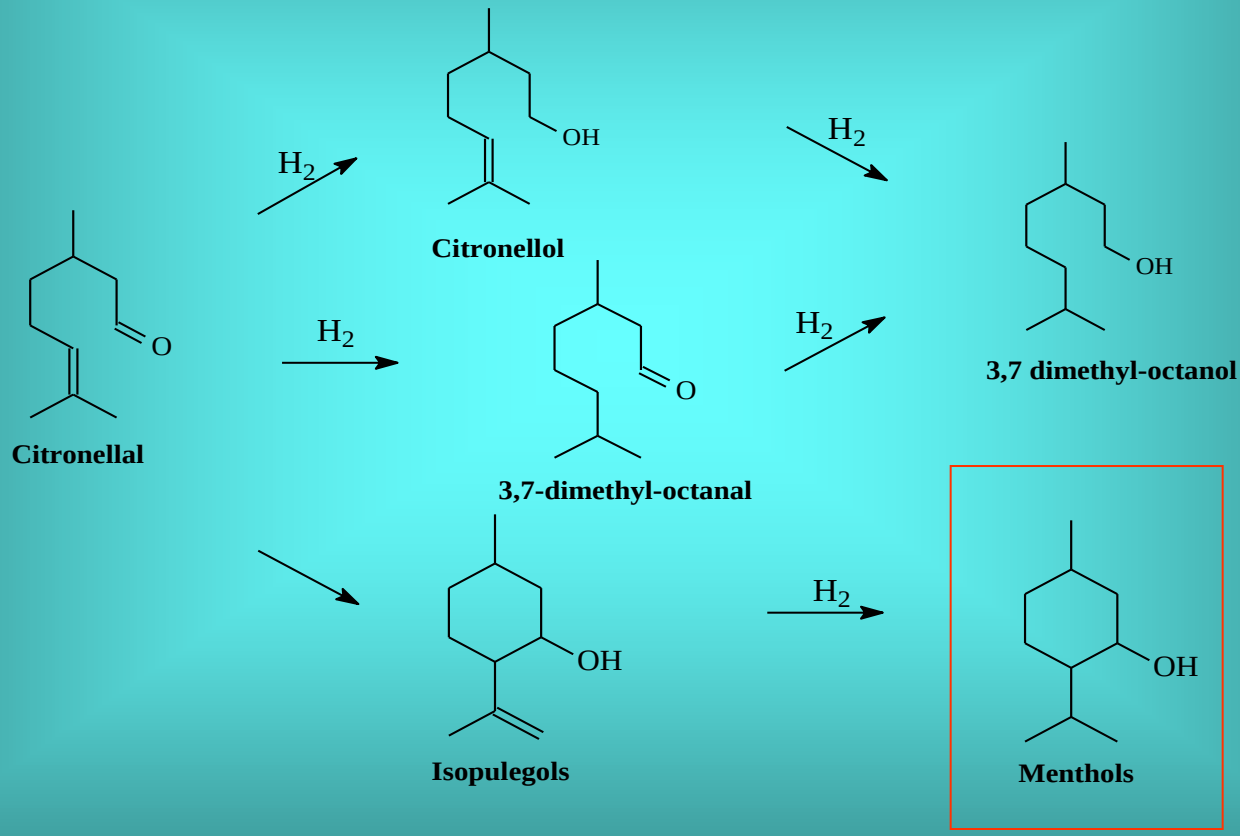

Chem. Commun., (2004) 1292-1293.

Citronellal hydrogenation

Influence of the metal loading and support

Ir/NaBeta25S

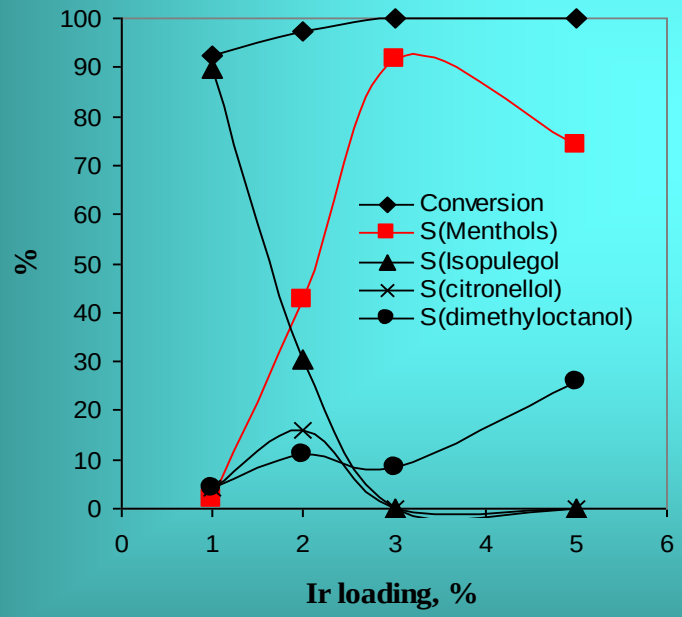

Ir/HBeta25

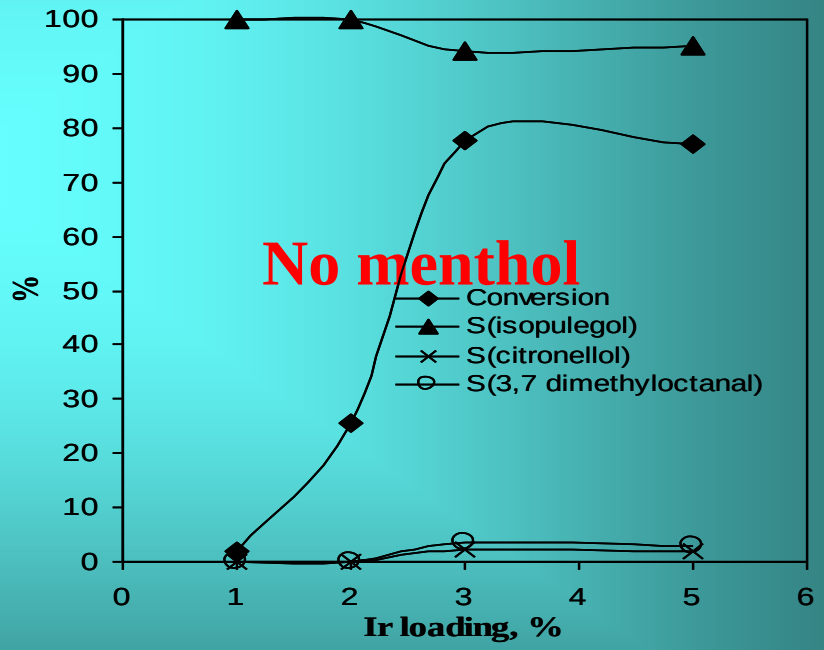

Reaction conditions:

0.8 MPa H_2, 80 C, cyclohexane, 10h

Chem. Commun., (2004) 1292-1293.

Citronellal isomerization

Influence of Ir and of the support

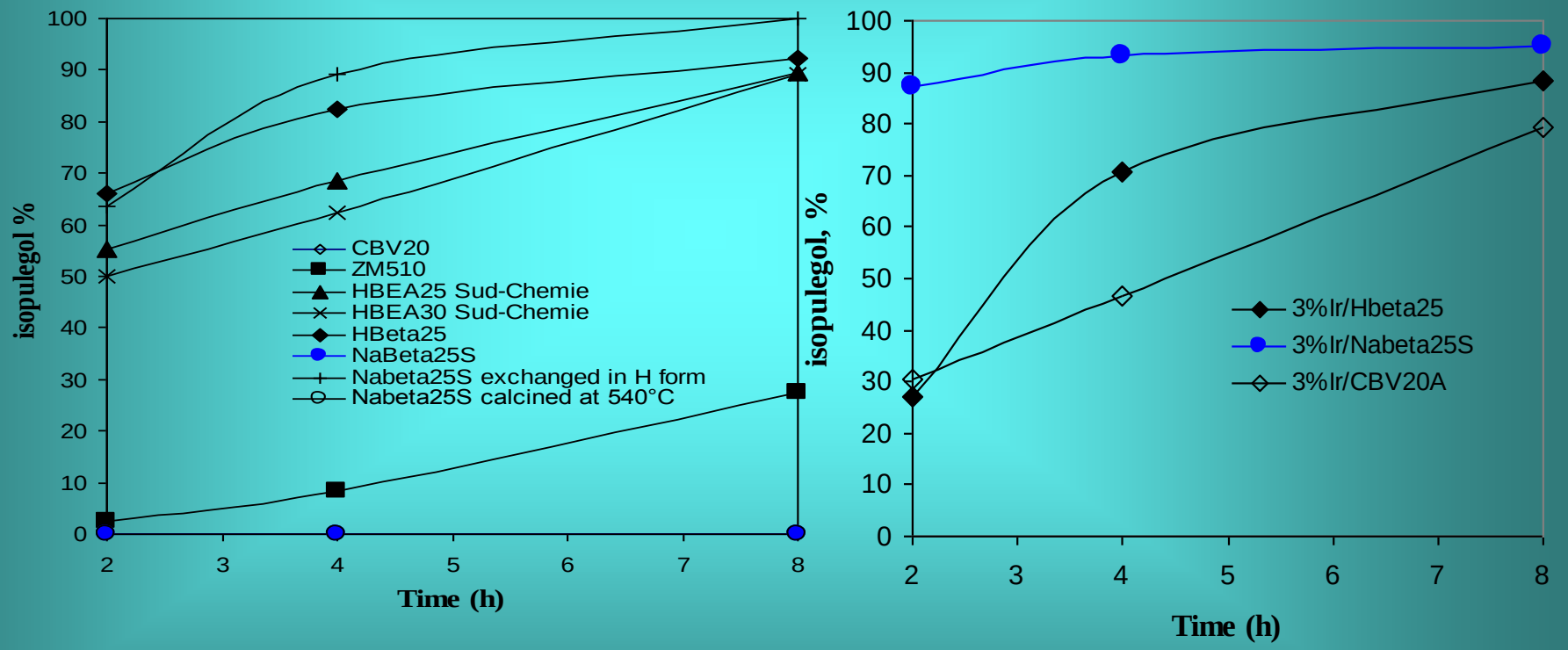

Reaction conditions:

80 C, cyclohexane

Chem. Commun., (2004) 1292-1293.

XPS Binding energies, and Ir^o/Ir^{n+} and Ir/Si(Zr) ratios

Catalyst	Binding energy of Ir levels, eV				Ir^o/Ir^{n+} ratio	Binding energy, eV			Comparative Ir/Si ratios x 10^3	
	Ir^0		Ir^{n+}							
	$Ir_{4f7/2}$	$Ir_{4f5/2}$	$Ir_{4f7/2}$	$Ir_{4f5/2}$		Si_{2p}	Al_{2p}	O_{1s}	Analytic	XPS
1%Ir/BEA	61.4	64.6	63.2	65.4	**0.56**	103.5	74.8	532.8	**3.3**	**6.0**
2%Ir/BEA	61.2	64.4	63.0	65.0	**1.26**	103.6	74.8	532.8	**6.6**	**11.2**
3%Ir/BEAS5	61.2	64.2	62.7	65.1	**1.68**	103.6	74.6	532.8	**9.9**	**20.6**
3%Ir/BEA-S	61.2	64.2	62.7	65.1	**1.70**	103.6	74.6	532.8	**9.9**	**20.6**
5%Ir/BEA	61.2	64.3	62.6	65.2	**1.84**	103.6	74.7	532.8	**16.5**	**42.1**

Chem. Commun., (2004) 1292-1293.

Fourier transforms of EXAFS

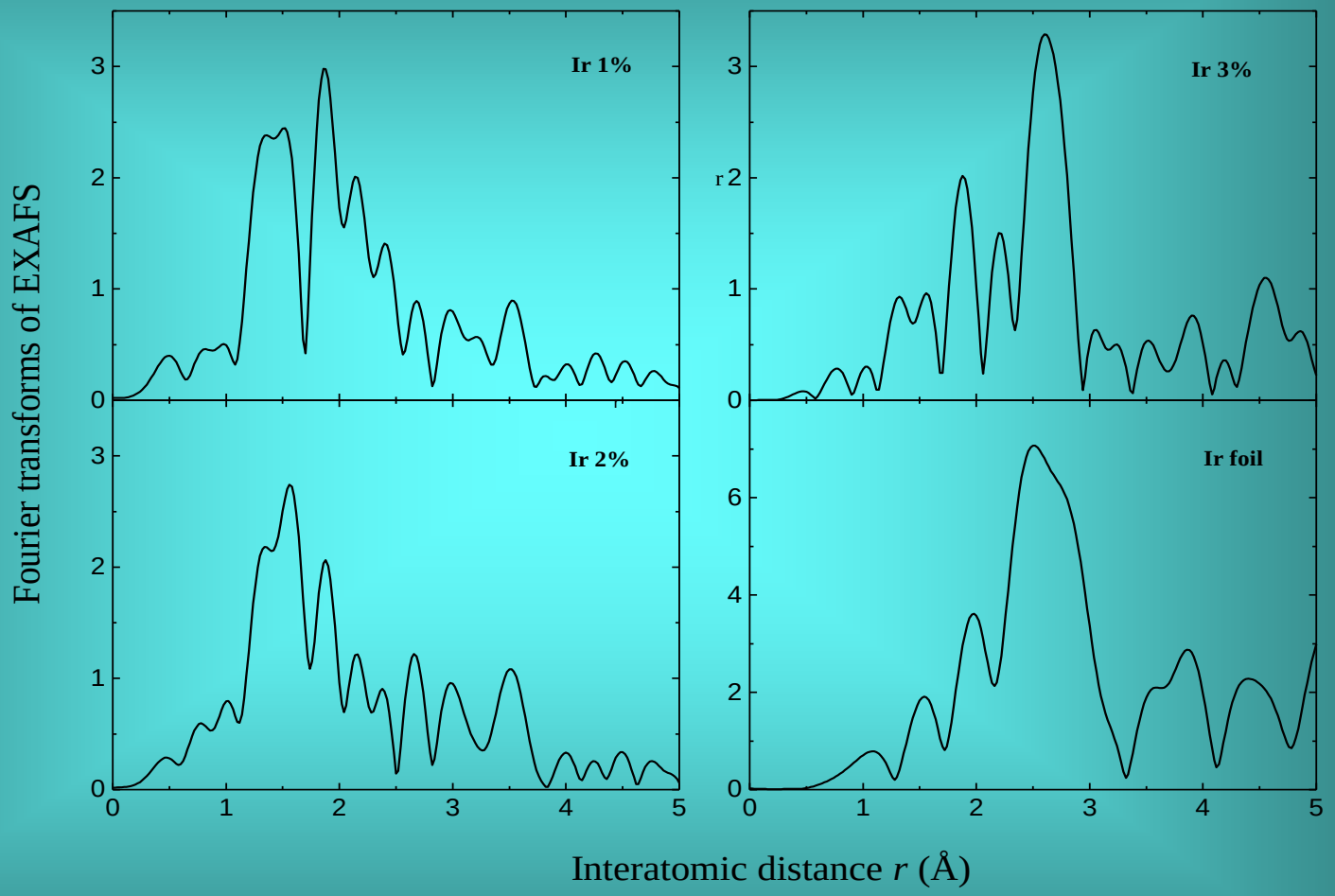

Chem. Commun., (2004) 1292-1293.

HRTEM- 1% Ir/Na-BEA-S

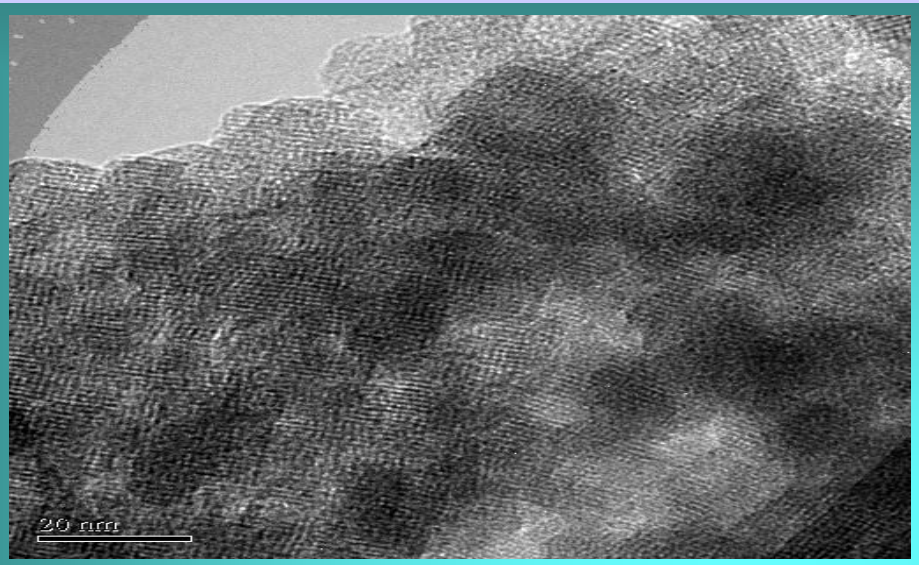

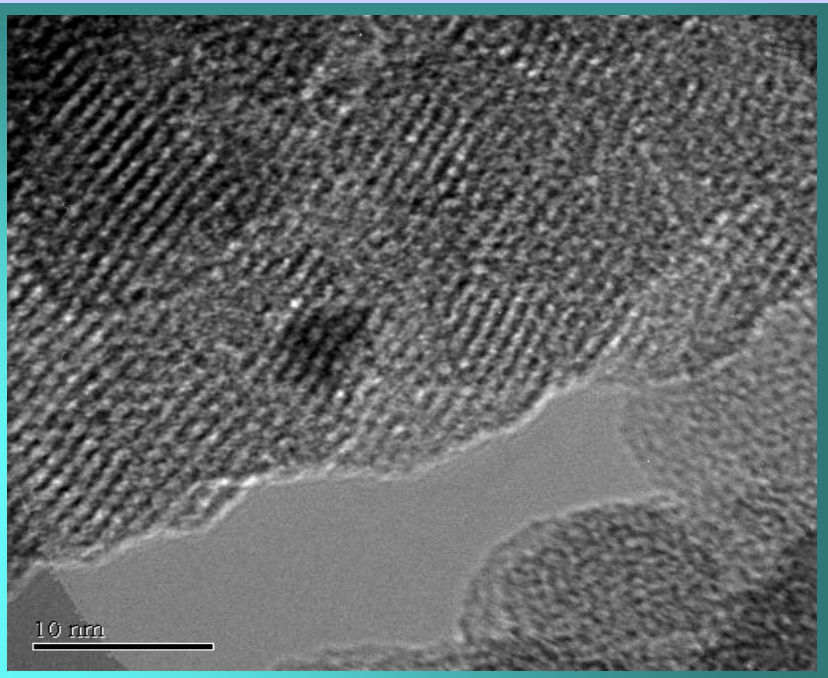

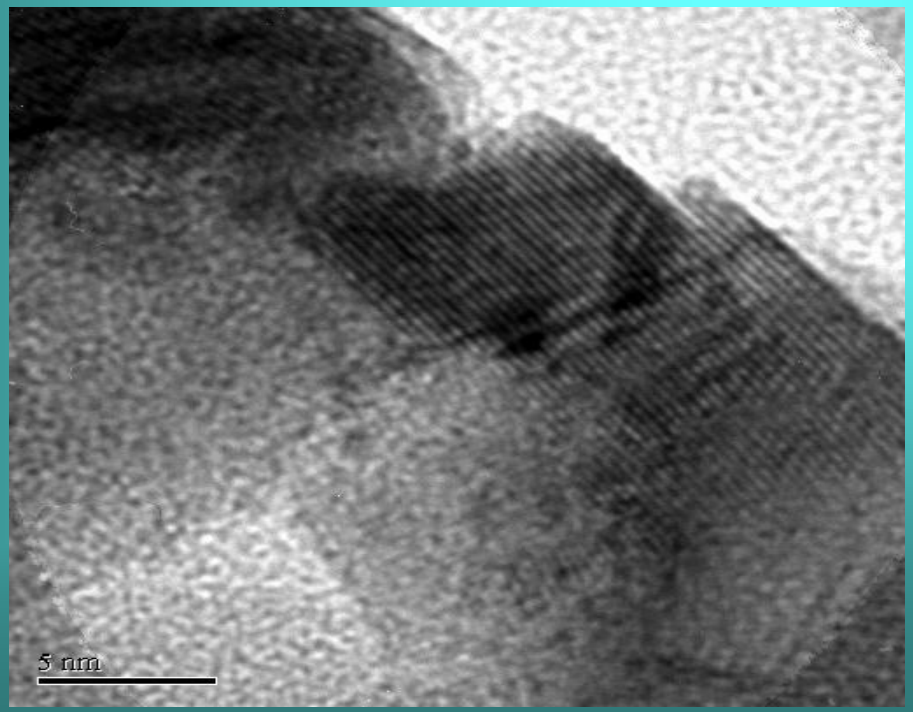

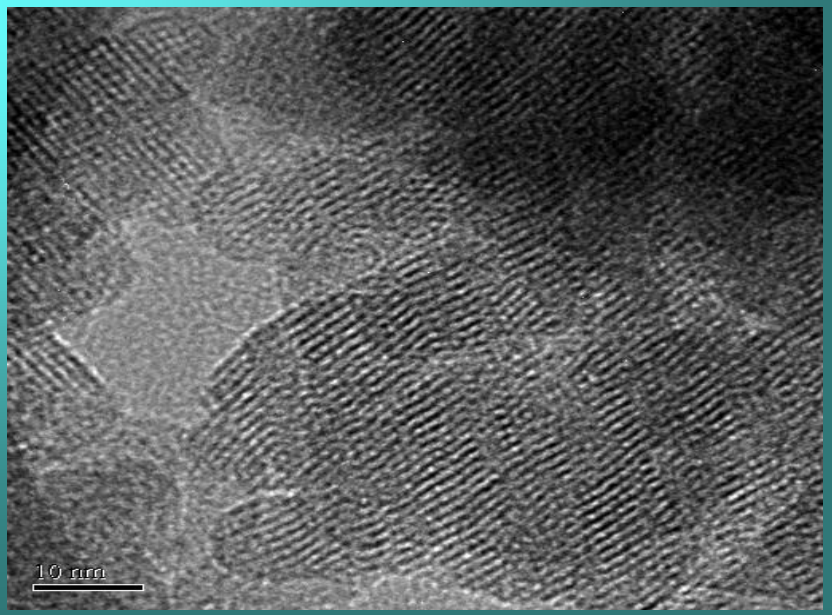

HRTEM- 3% Ir/Na-BEA-S

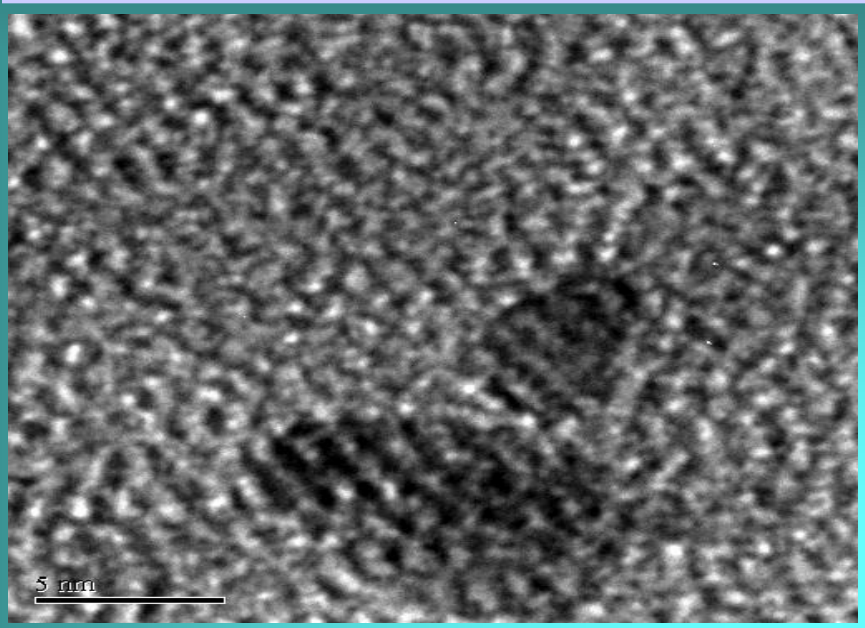

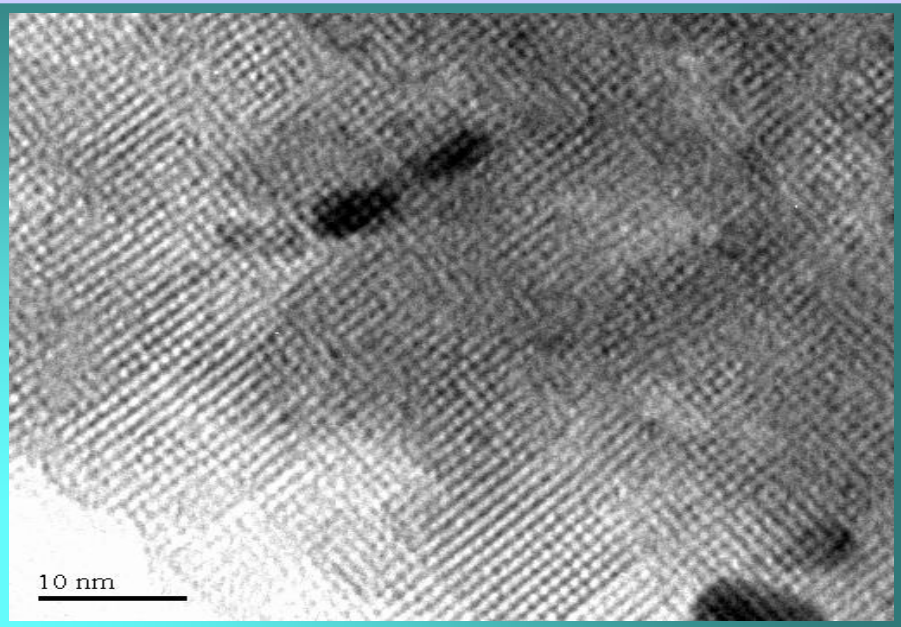

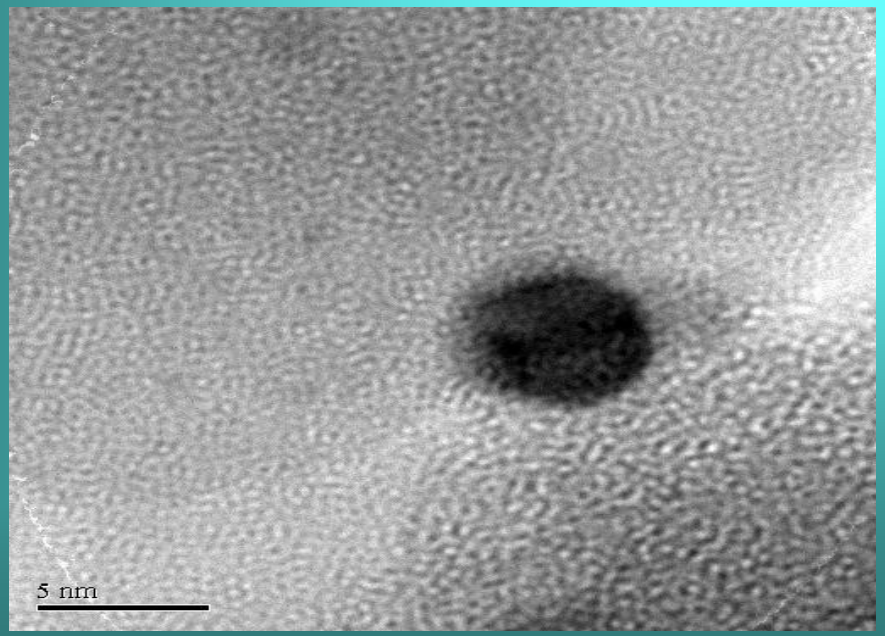

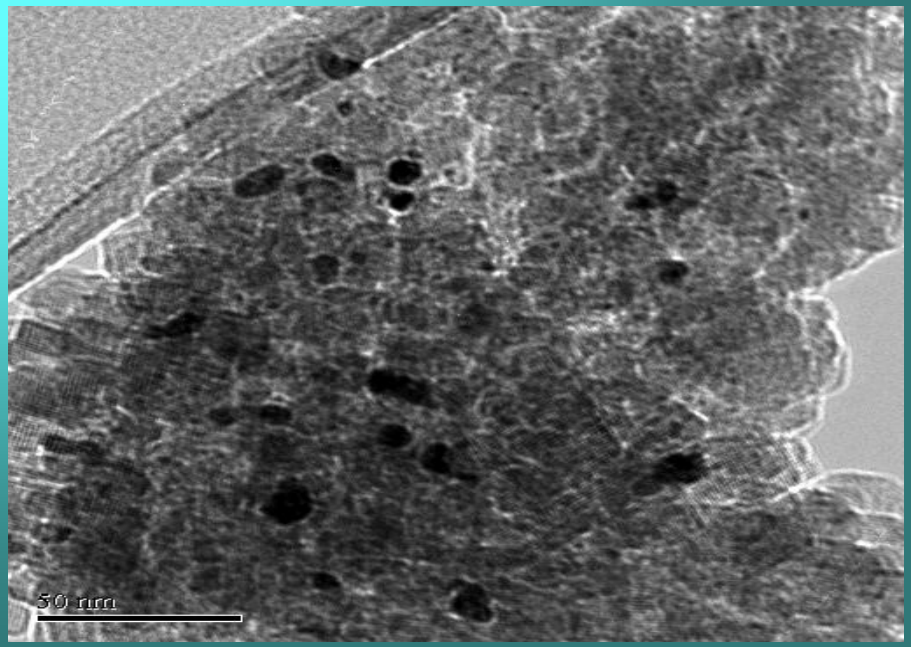

Deposition-precipitation

How the story starts?

Echavarren suggested that gold could be an efficient catalyst for coupling reactions

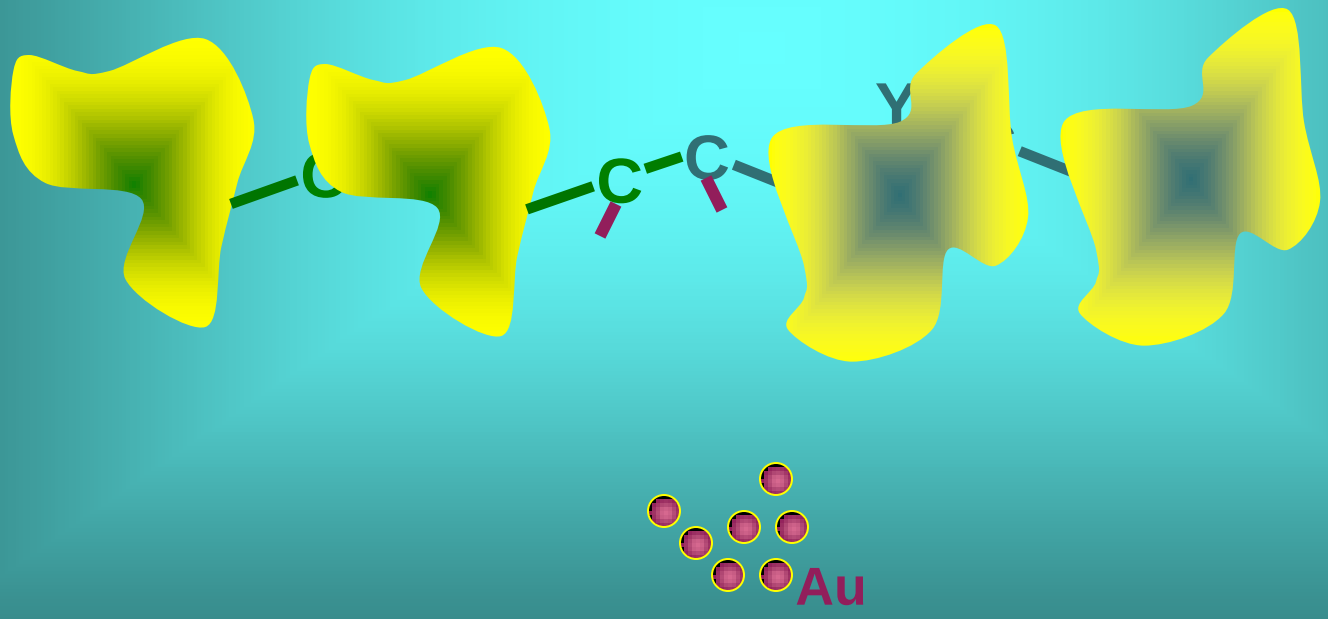

C. Nieto-Oberhuber, S. Lopez, A. M. Echavarren, *J. Am. Chem. Soc*. 127 (2005) 6178

Why not to use gold for cycloisomerisation reactions to obtain heterocycles?

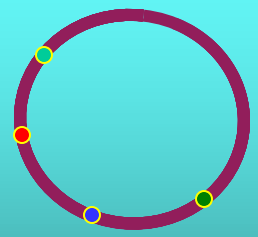

What kind of heterocycles?

A **lactone** is a cyclic ester in organic chemistry

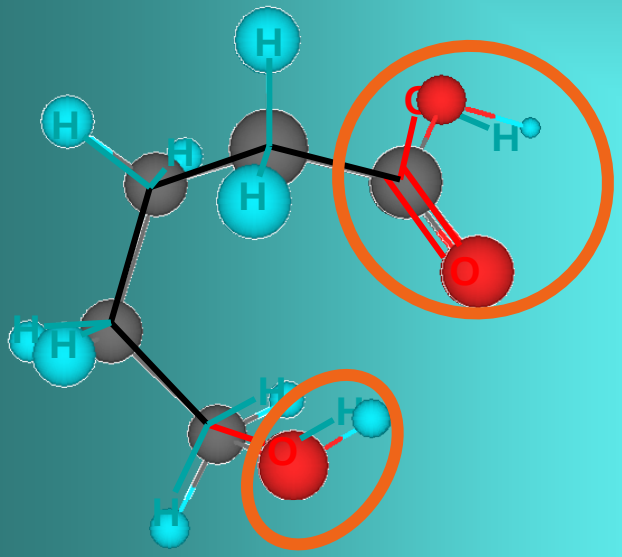

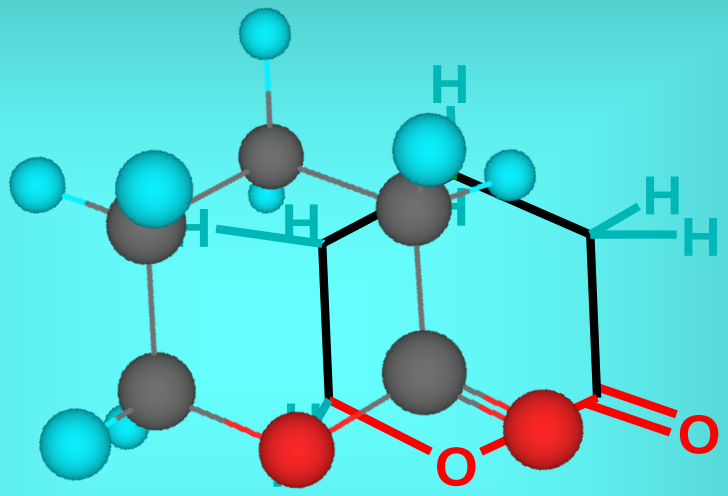

… and it is the condensation product of an alcohol group and a carboxylic acid group in the same molecule.

Importance of lactones

Lactones are found in various forms in numerous naturally occurring compounds.

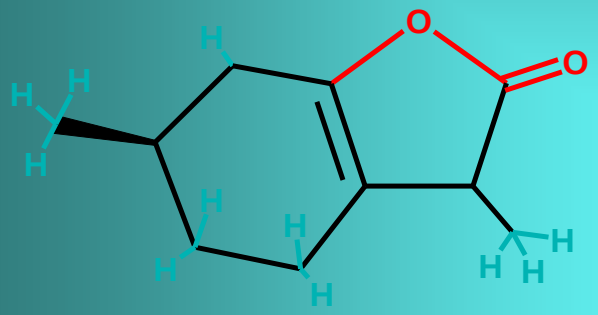

Unsaturated γ-lactone rings

are present in many components of essential oils

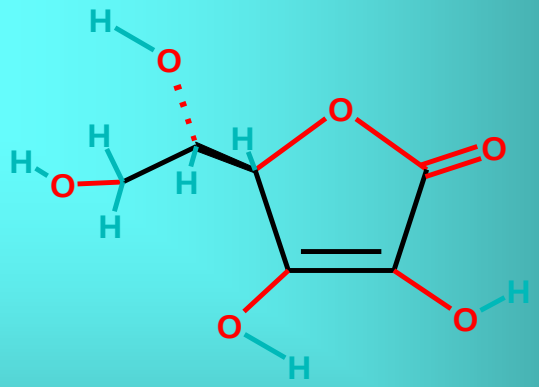

vitamin C

is a carbohydrate lactone

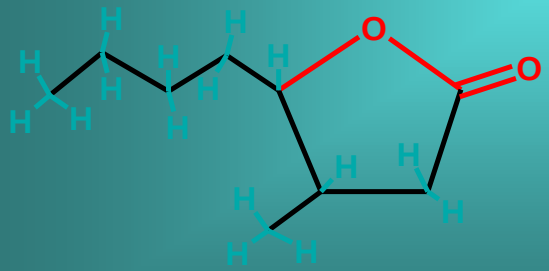

whisky lactone

is found in oak trees, and impart flavor to whisky

How they have been synthesized?

- by conventional Lewis acids
- toxic Hg salts
- Pd, Ru, Rh, Ni, Ag, Zn

Conditions:

elevated temperatures

additives or ligands or/and strong base

refluxing solvents

Why we should use gold?

- mild conditions, no additives

Gold homogeneous catalysis

Unsubstituted substrate

96%

Conditions: **10 mol% AuCl**

acetonitrile

RT, 1h

K_2CO_3

H. Harkat, J.-M. Weibel, P. Pale, *Tetrahedron Letters*, 2006, 47, 6273

Gold homogeneous catalysis

Substituted substrate

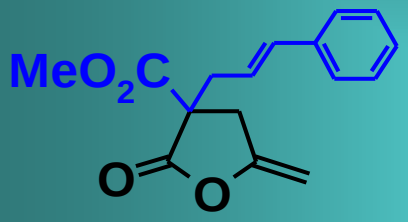

90%

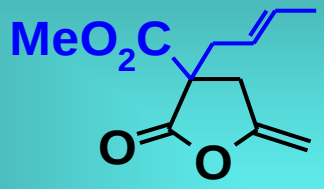

78%

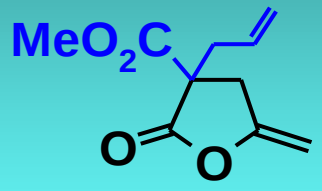

72%

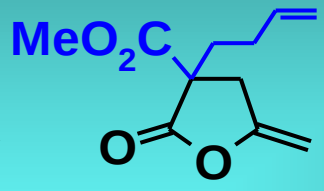

87%

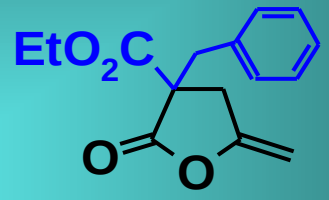

97%

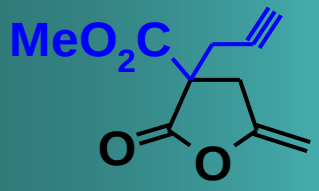

97%

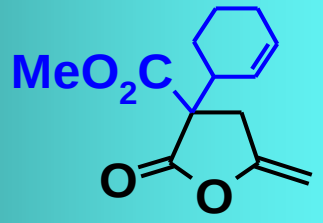

89%

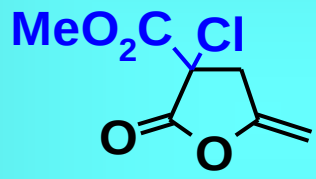

97%

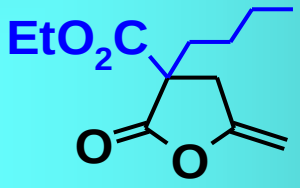

83%

Conditions: **5 mol% AuCl or $AuCl_3$**

acetonitrile

RT, 2h

No use of a base

E. Genin, P. Y. Toullec, S. Antoniotti, C. Brancour, J.-P. Genet, V. Michelet, *JACS*, 2006, 128, 3112

Gold homogeneous catalysis

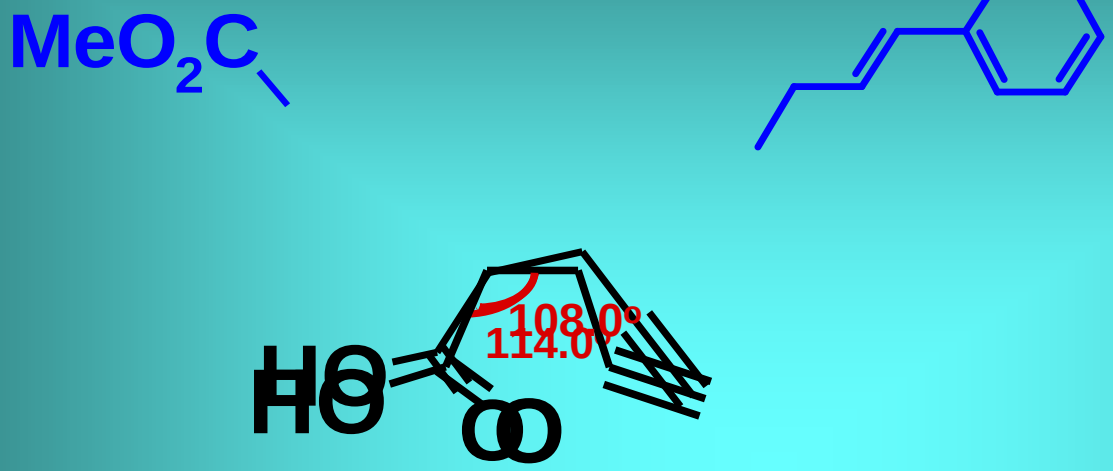

Conditions: 5 mol% AuCl or $AuCl_3$

acetonitrile

RT, 2h

No use of a base

E. Genin, P. Y. Toullec, S. Antoniotti, C. Brancour, J.-P. Genet, V. Michelet, *JACS*, 2006, 128, 3112

? Heterogeneization by gold- ionic exchange?

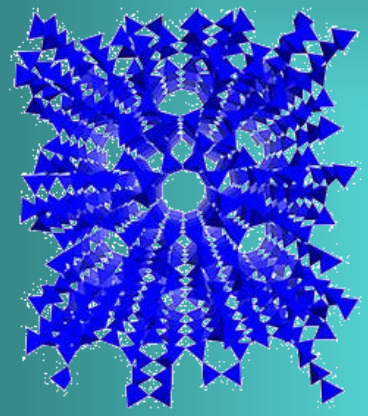

ZSM-5

or

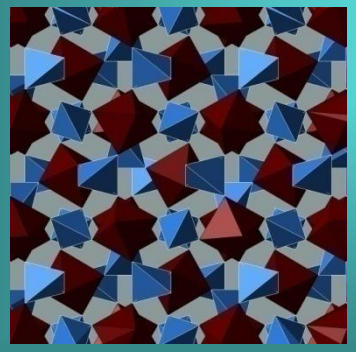

Beta zeolite

+ AuCl or $AuCl_3$

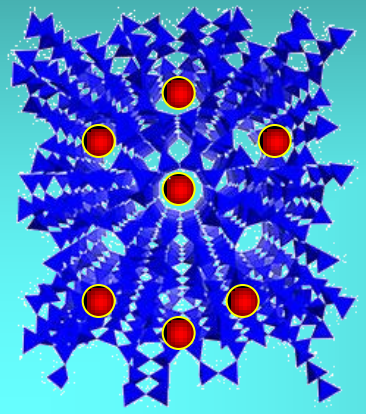

0% conversion

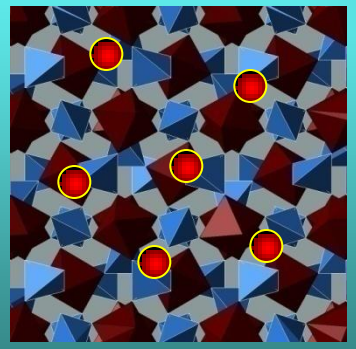

0% conversion

How heterogenize the gold system?

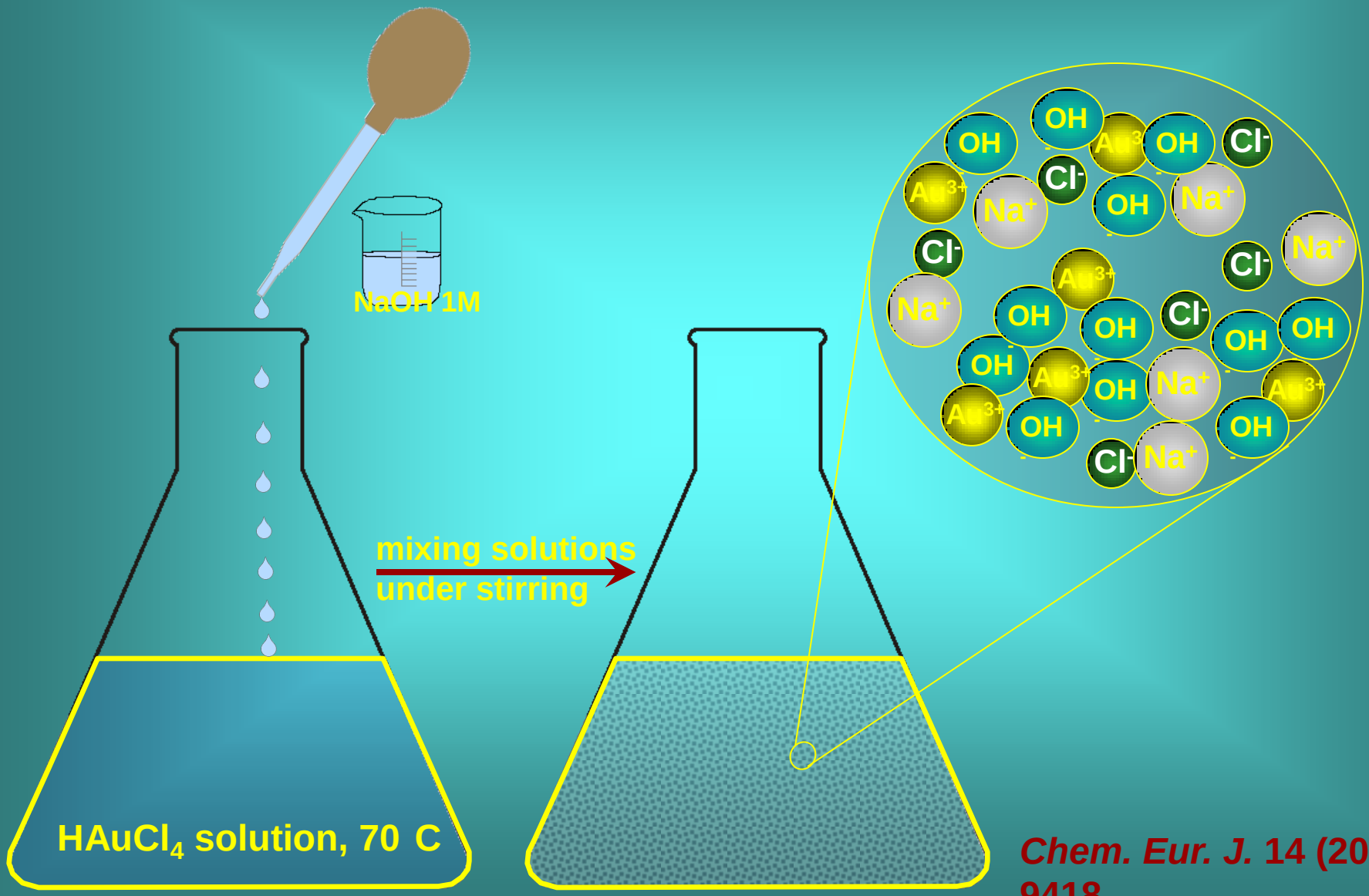

Chem. Eur. J. 14 (2008) 9412-9418.

How heterogenize the gold system?

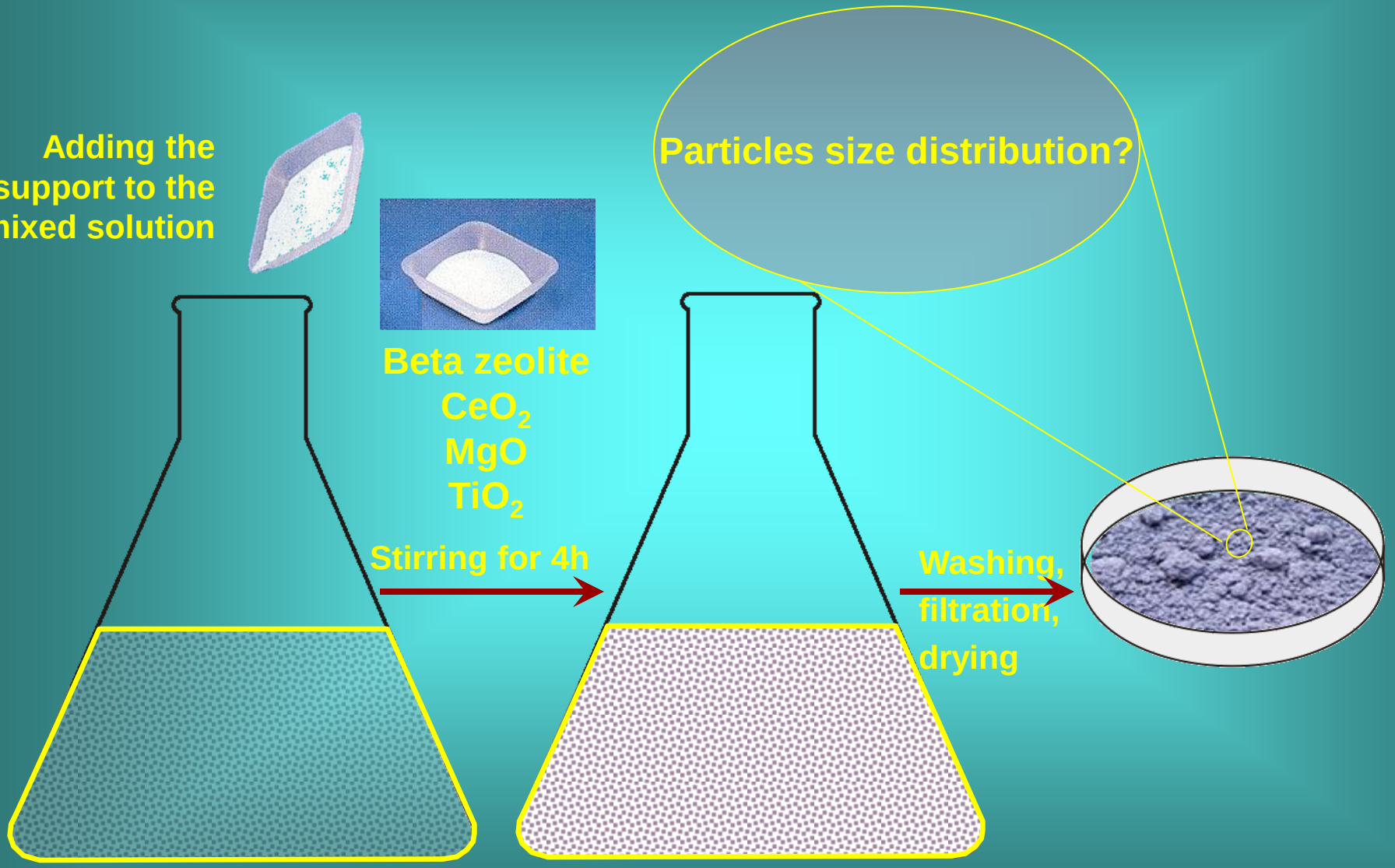

A. Corma, P. Serna, *Science* 2006, *313,* 332 and references herein

S. Carrettin, J. Guzman, A. Corma *Angew. Chem. Int. Ed.* 2005, *44*, 2242-2245

Catalytic tests

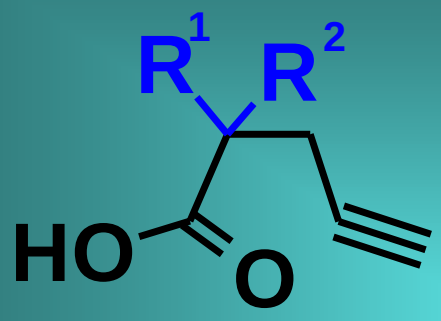

Gold catalyst, CH_3CN

8h, RT-40 C

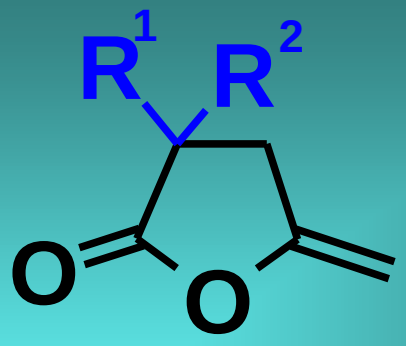

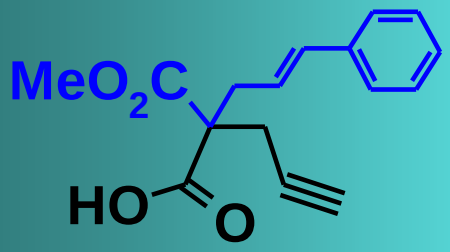

Substituted acetylenic acid, reactive

		Conversion	Isolated yield
Au/CeO_2	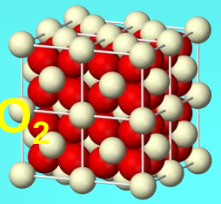	0%	/
Au/MgO	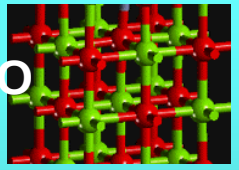	0%	/
Au/TiO_2	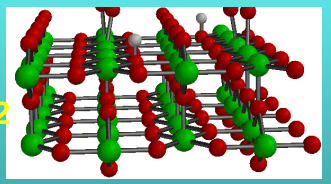	50%	25%
Au/Beta zeolite	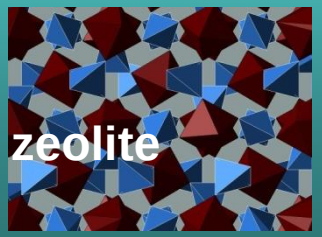	100%	99%

Chem. Eur. J. 14 (2008) 9412-9418.

TEM images and EDX analysis of Au/zeolite beta

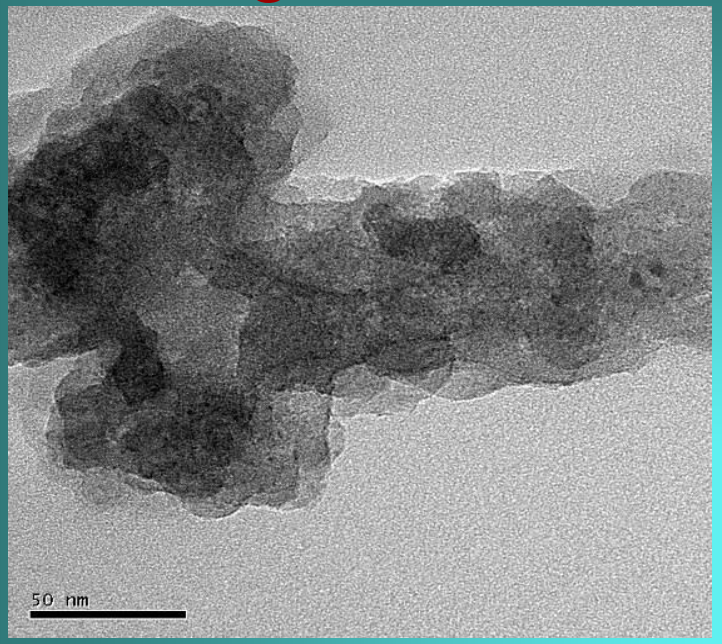

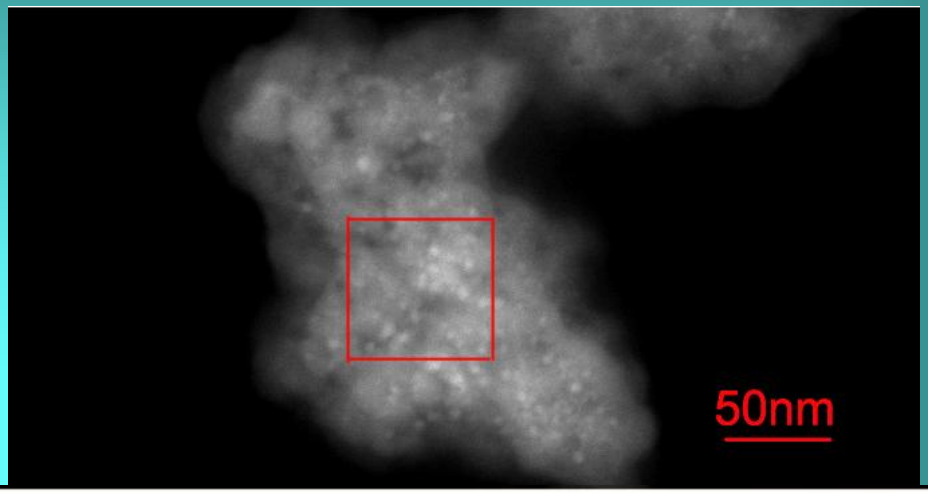

quite narrow
size distribution
3-4 nm

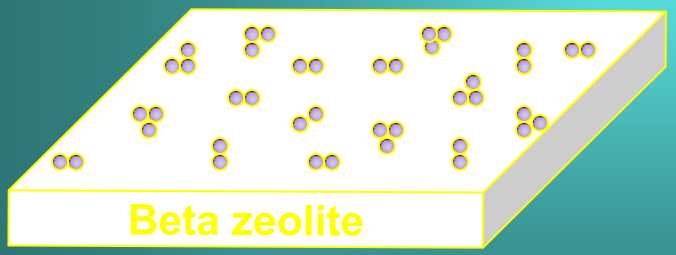

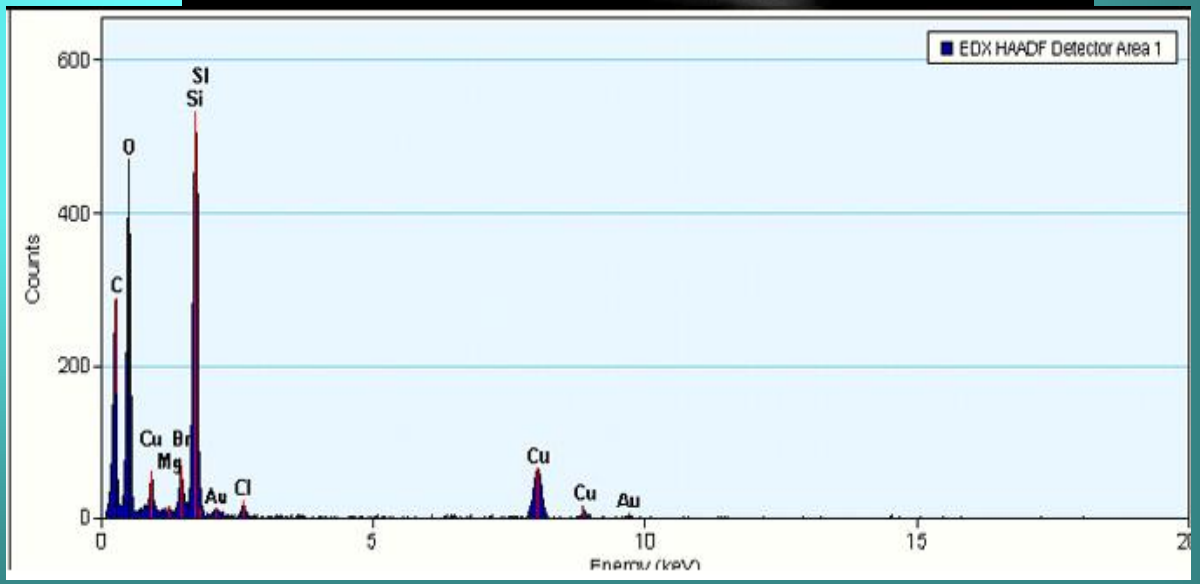

F. Neaţu, Z. Li, R. Richards, P. Y. Toullec, J.-P. Genêt, K. Dumbuya, J. M. Gottfried, H.-P. Steinrück, V. I. Pârvulescu, V. Michelet, *Chem. Eur. J.* 14 (2008) 9412-9418.

TEM images and EDX analysis of Au/MgO

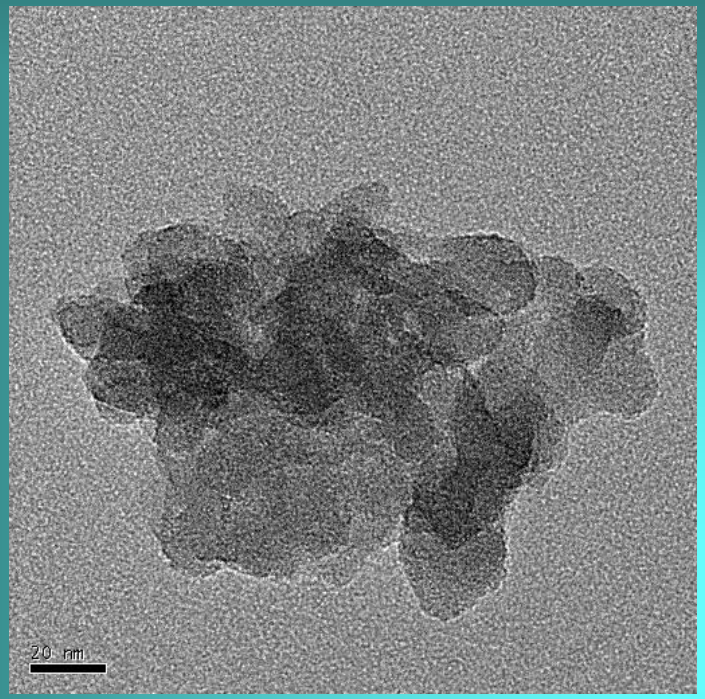

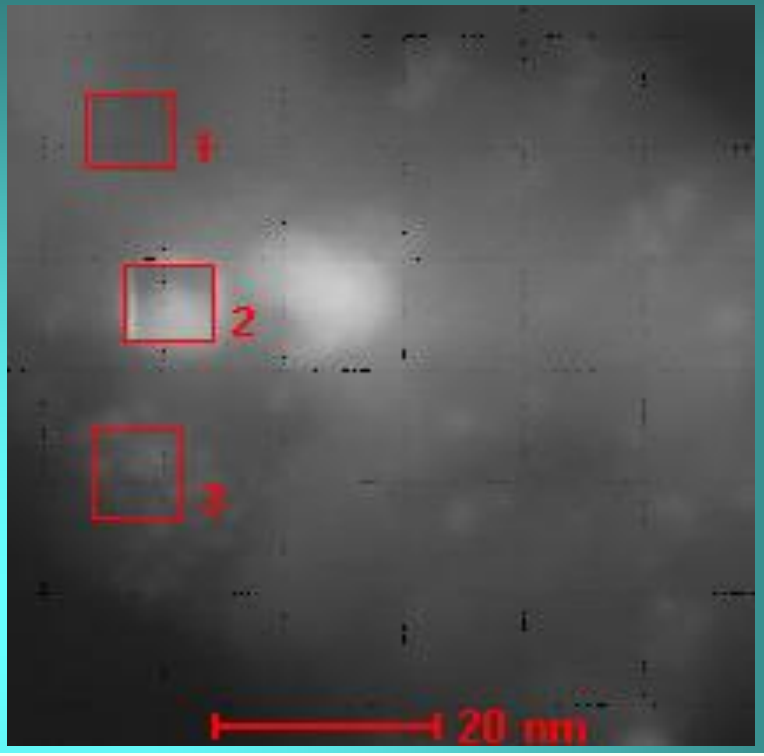

structural non-uniformities 3-12 nm

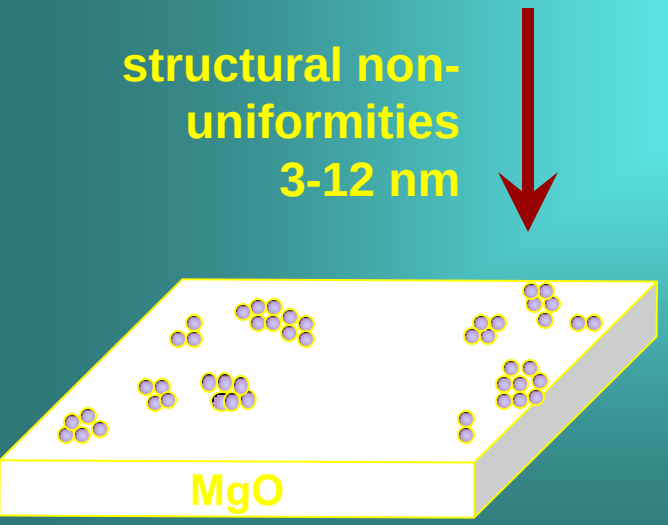

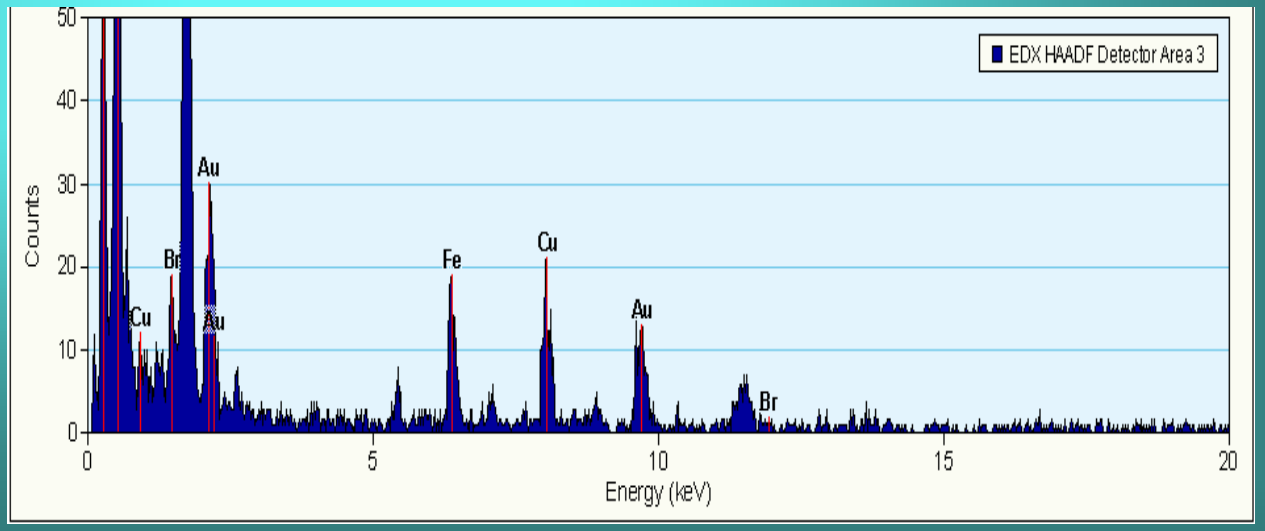

Chem. Eur. J. 14 (2008) 9412-9418.

Surface area and average particle size of supported catalysts

Catalyst	Au loading [wt.%]	Surface area [m^2g^{-1}]	Average Au particle size [nm]*
beta	-	464	
Au/beta	**4**	**383**	**3-5**
Au/CeO_2	4	82	5-12
Au/MgO	2	62	3-12
Au/TiO_2	4	42	5-8

*measured from TEM

Chem. Eur. J. 14 (2008) 9412-9418

Catalytic tests

Au/Beta zeolite

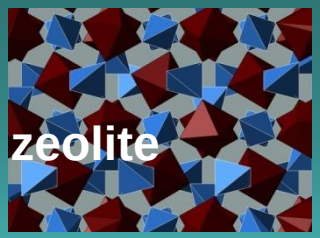

Substituted acetylenic acid

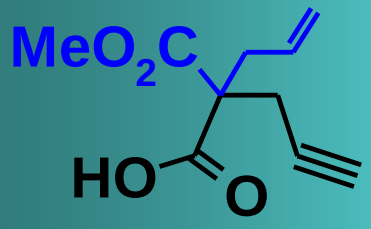

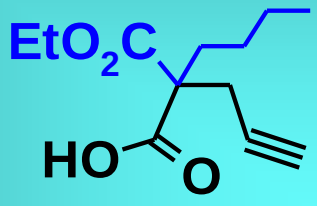

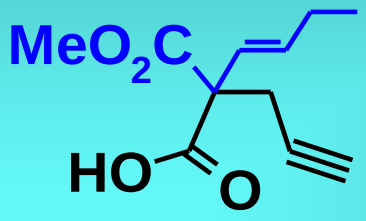

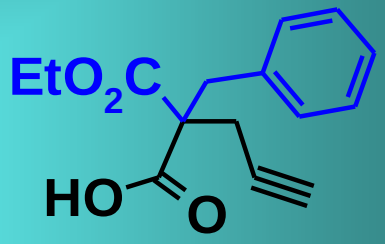

40 C **88% (100%)** **85% (100%)** **80% (100%)** **71% (100%)**

Very good results, comparable with the results obtained in homogeneous catalysis.

RT **60% (90%)** **65% (70%)**

Performing the reaction at room temperature corresponded to smaller reaction rates

Yield% (Conv.%)

***Chem. Eur. J.* 14 (2008) 9412-9418**

Catalytic tests

$AuCl_3$, without base, homogeneous catalysis

Unsubstituted acetylenic acid

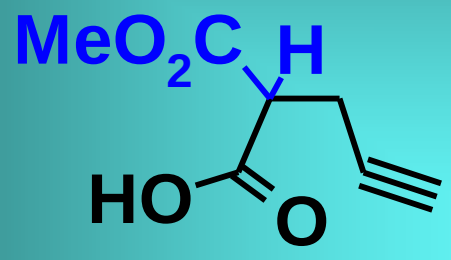

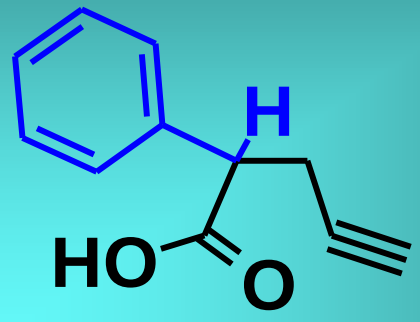

40 C	0% (0%)	0% (0%)
RT	0% (0%)	0% (0%)

NO REACTION

Yield% (Conv.%)

V.I. Pârvulescu et al., *Chem. Eur. J.* 14 (2008) 9412-9418

Catalytic tests

Au/Beta zeolite

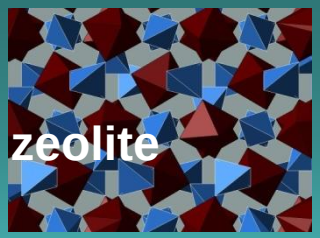

Unsubstituted acetylenic acid

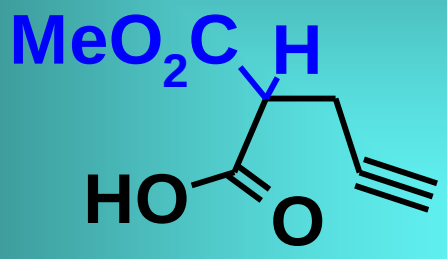

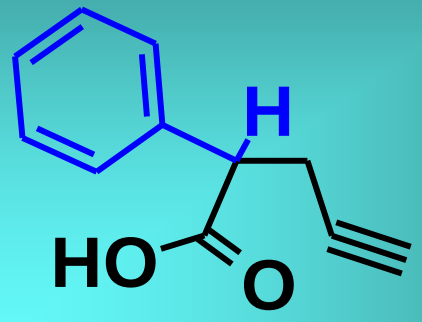

40 C — **50% (100%)** — **80% (85%)**

Possible decomposition of the product

RT — **25% (40%)** — **12% (30%)**

Performing the reaction at room temperature corresponded to smaller reaction rates

Yield% (Conv.%)

Chem. Eur. J. **14 (2008) 9412-9418**

Performing the reaction in *ARGON* atmosphere gave much LOWER results then performing reaction in AIR.

WHY?

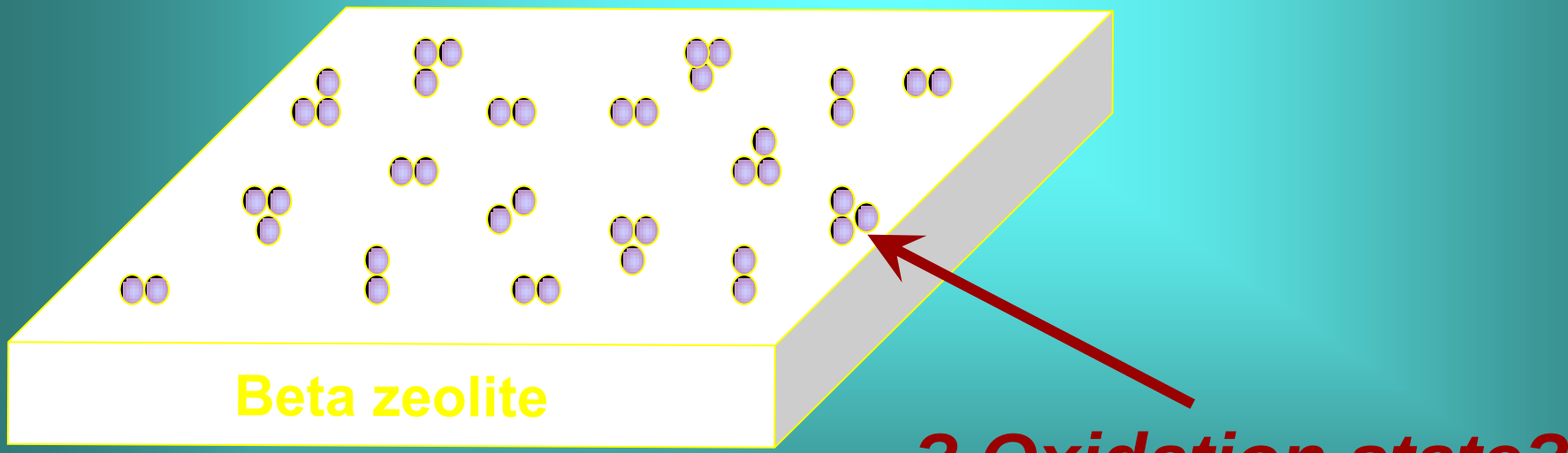

In-situ high-pressure XPS of the Au/beta catalyst

Argon

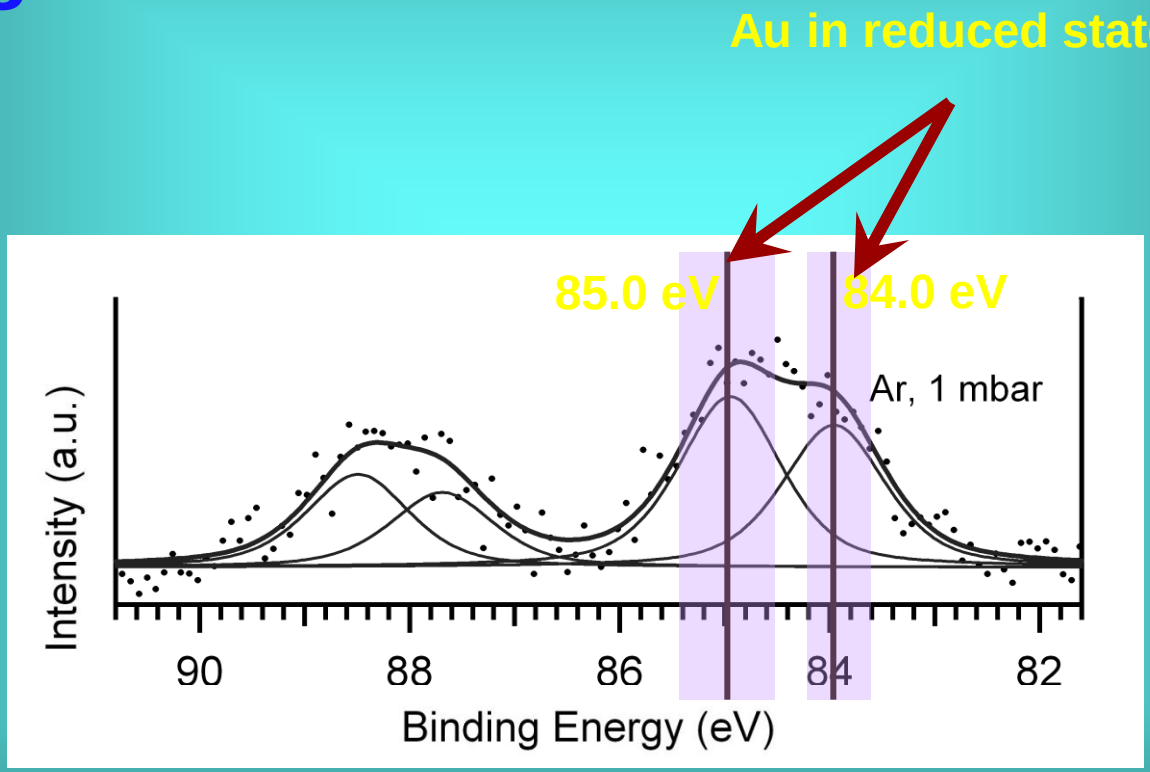

Chem. Eur. J. 14 (2008) 9412-9418

In-situ high-pressure XPS of the Au/beta catalyst

- *No change observed when using a reducing species- like CO*
- *Even the initial sample was preserved in atmosphere conditions, the gold was reduced in the vacuum chamber of the XPS.*
- *No further reduction of Au(I) to Au (0) in the presence of CO, could be due to the Au species is incorporated into the zeolite framework .*

Au in reduced state (Au I)

CO

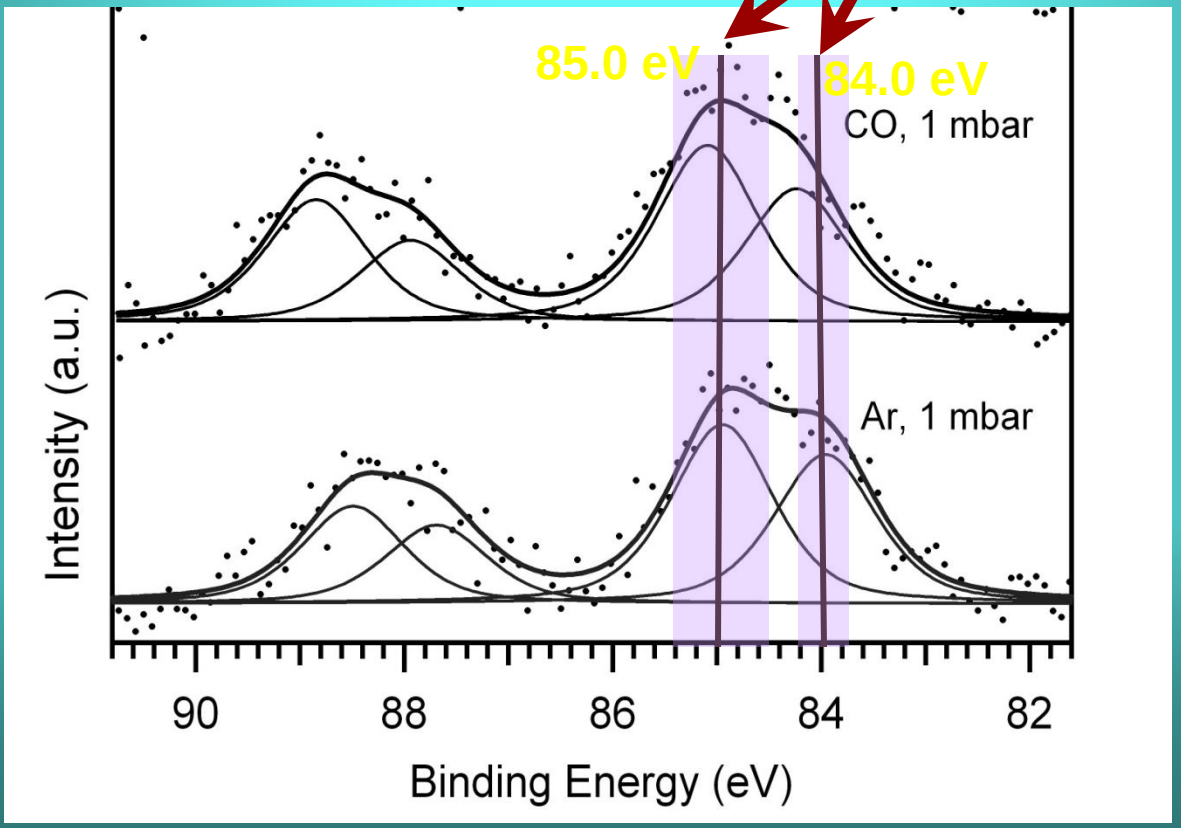

In-situ high-pressure XPS of the Au/beta catalyst

Oxygen

Au in oxidized state (Au III)

Au in reduced state (Au I)

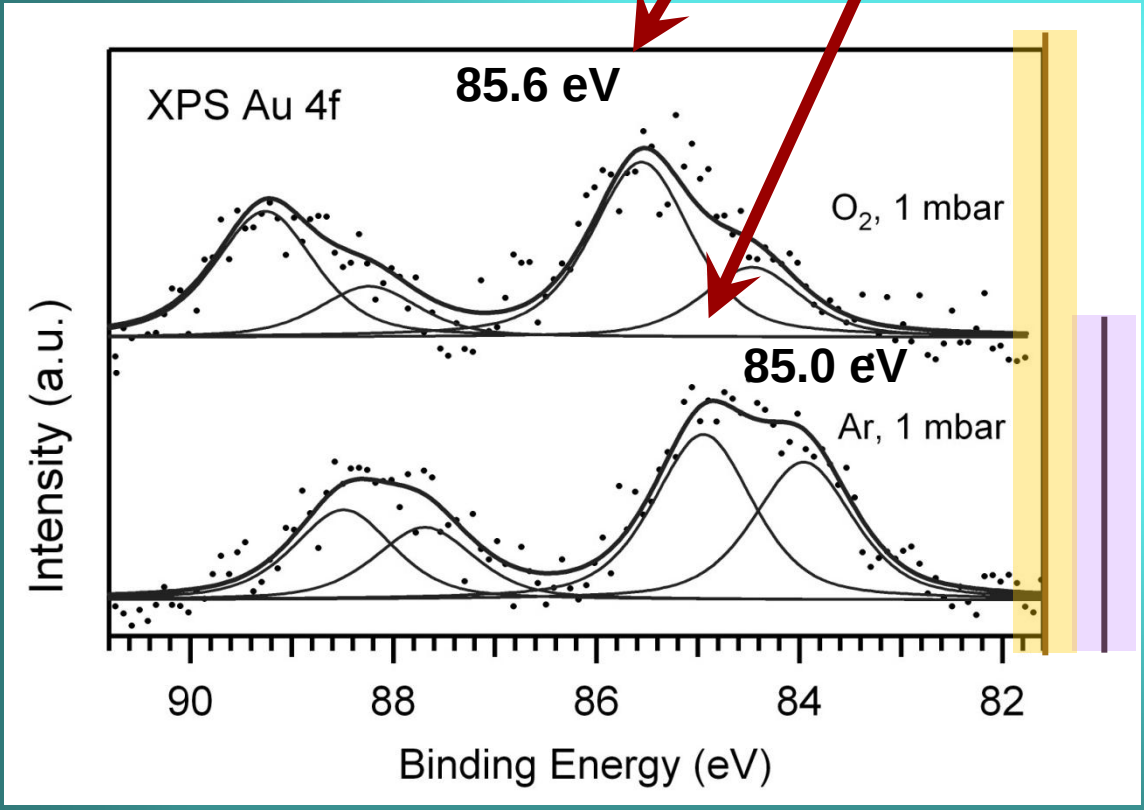

The reduction of the active site Au(III) to Au(I) in the presence of the acetylenic acid substrate is leading to inactive catalysts. The role of air is to reoxidize the inactive site Au(I) to the active site Au(III).

Chem. Eur. J. 14 (2008) 9412-9418

Recycling of the heterogeneous gold catalyst

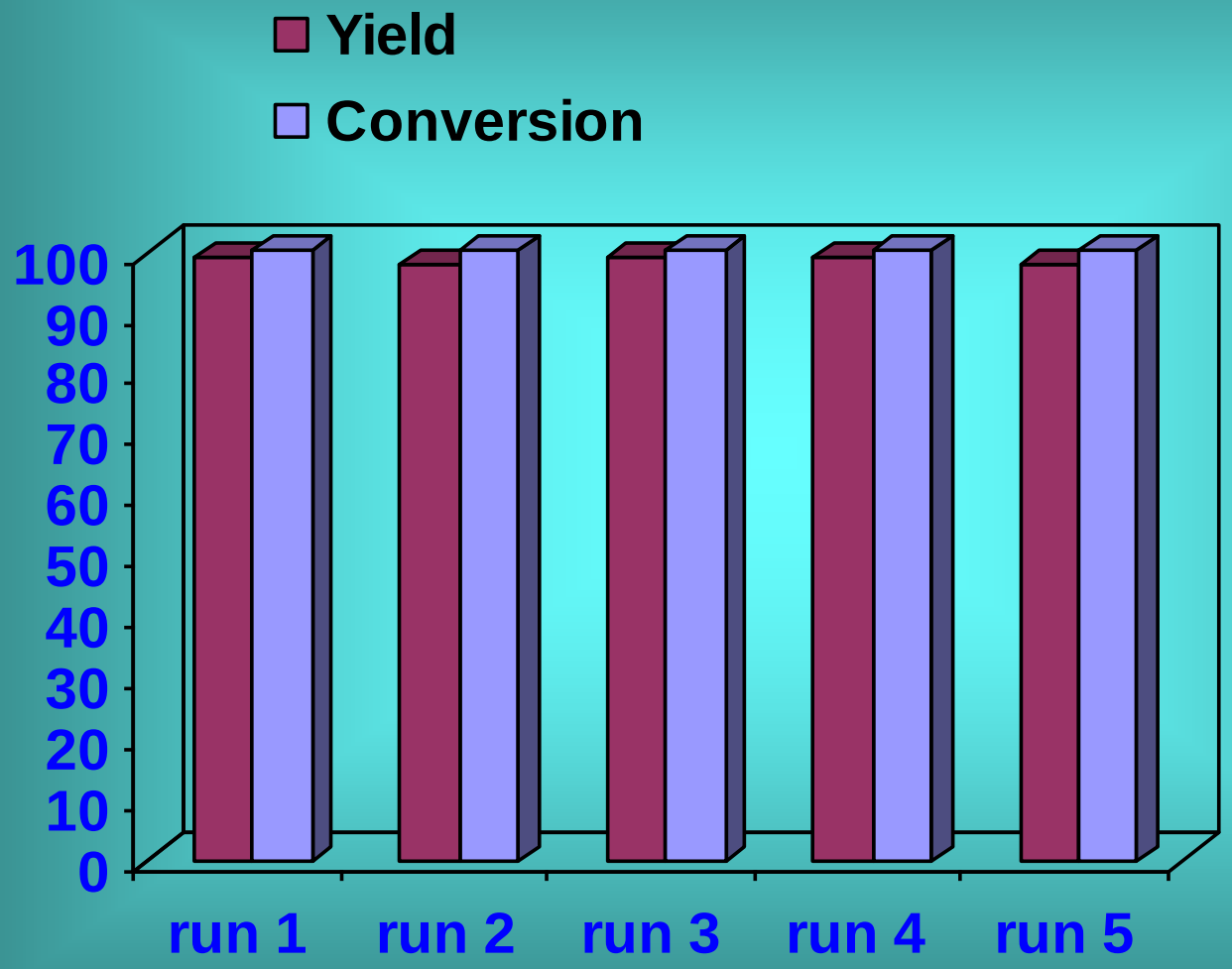

Chem. Eur. J. 14 (2008) 9412-9418

The colloid concept

Precursor concept to heterogeneous catalysts

$uMX, + vM'(BR_3H)_u \rightarrow uM\downarrow + vM'(BR_3X), + uv/2H_2\uparrow$

M= metal powder; M' =alkali or alkaline earth metal;

$R=C_1\text{-}C_8$ (alkyl); X= OH, OR, CN, OCN, SCN.

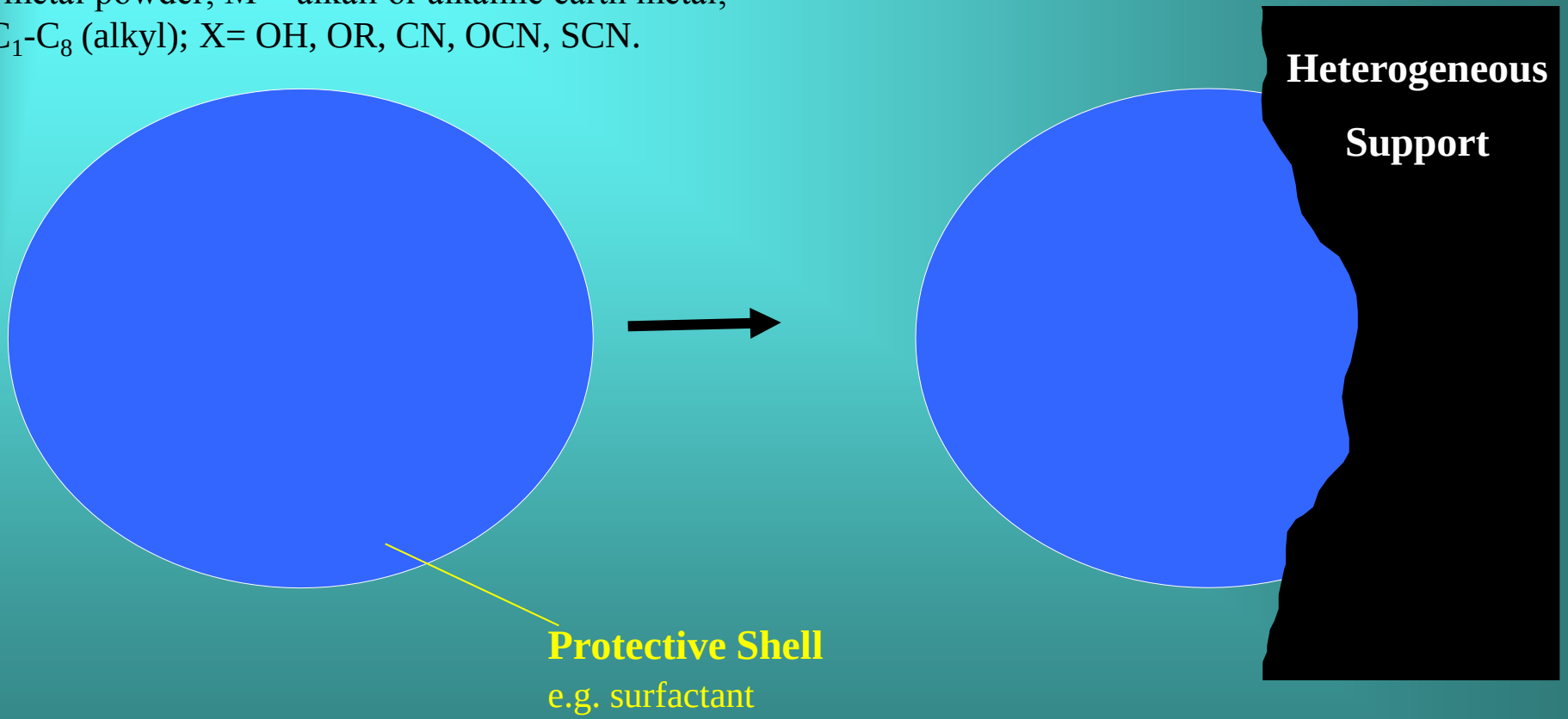

H. Bönnemann, W. Brijoux, Advanced Catalysts and Nanostructured Materials (Ed.: W. R. Moser), Academic Press, San Diego, 1996, p. 165.

H. Bönnemann and R. Richards, *Eur. J. Inorg. Chem.* **2001**, 2455-2480

Hidrogenolysis

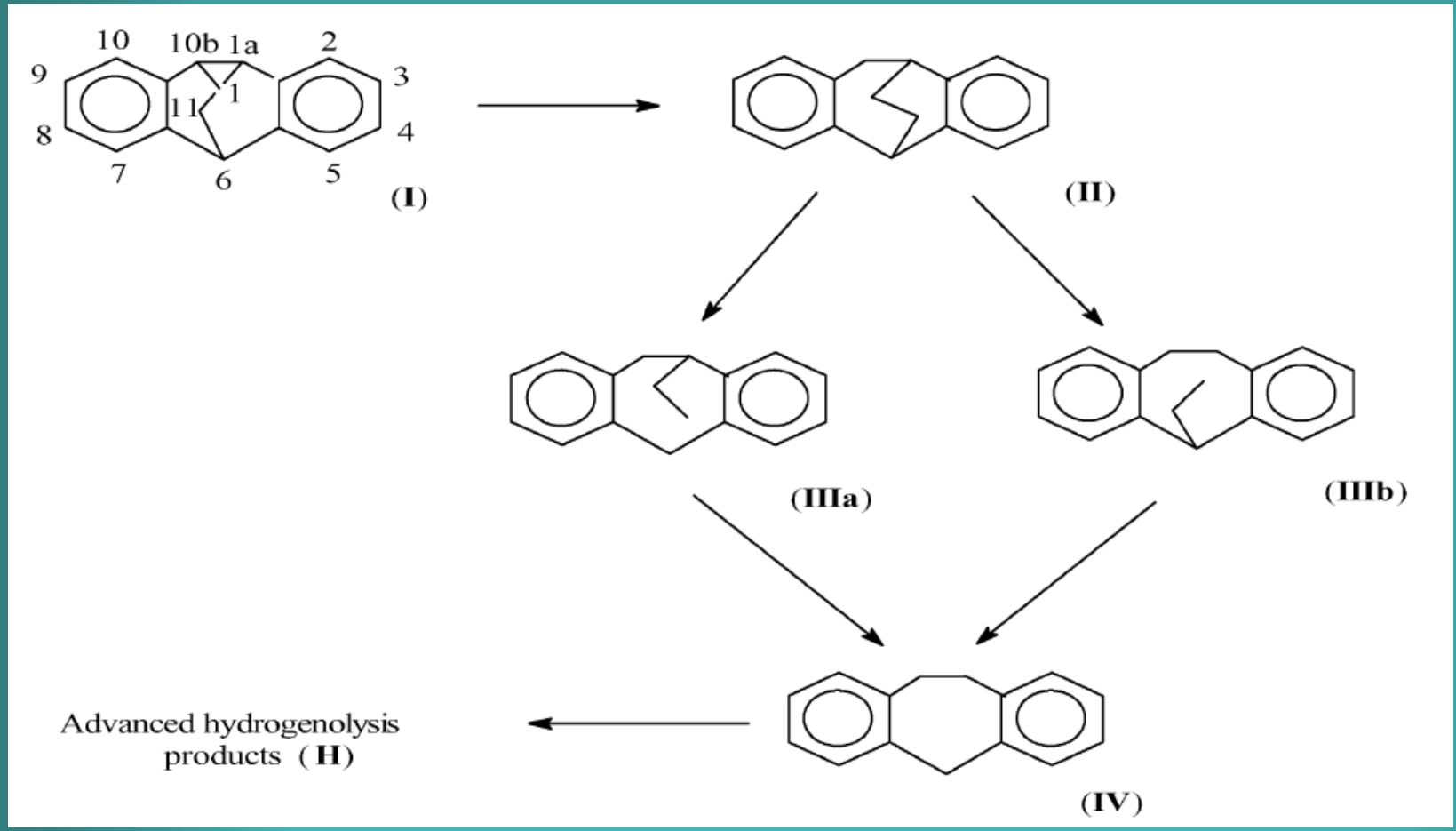

1,1a,6,10b-tetrahydro-1,6-methanodibenzo[*a*,*e*]cyclopropa[*c*]-cycloheptene over silica- and zirconia-embedded Ru-colloids

J. Mol. Catal., 178 (2002) 79-87; J. Mol. Catal. A: Chemical, 186 (2002) 153-161.

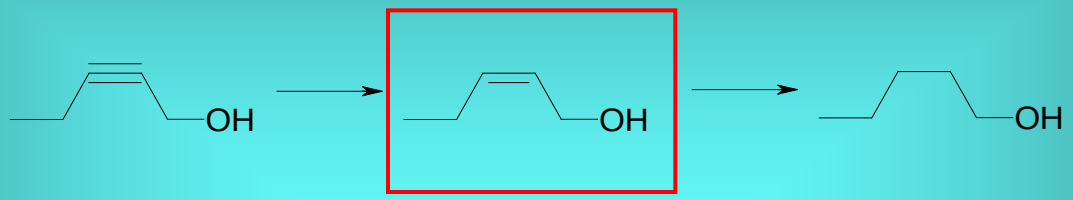

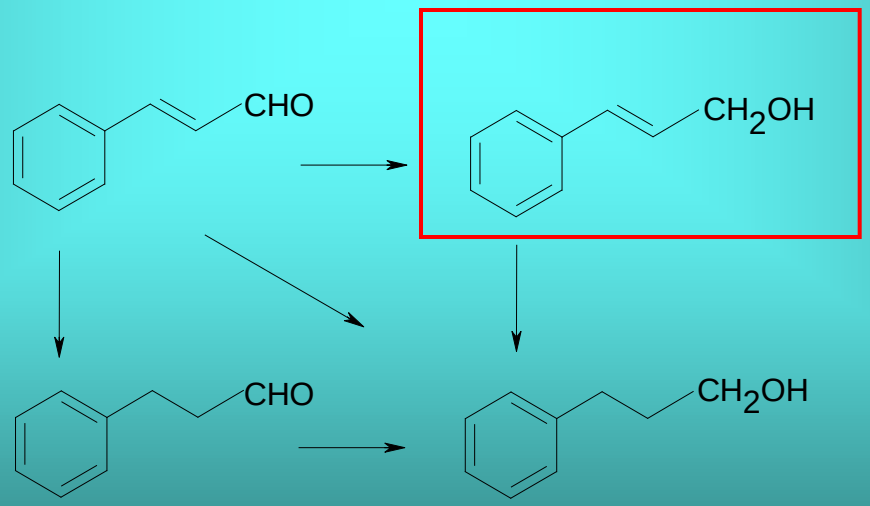

Chem Ind., 82 (2001) 301-306.

Nanoalloys

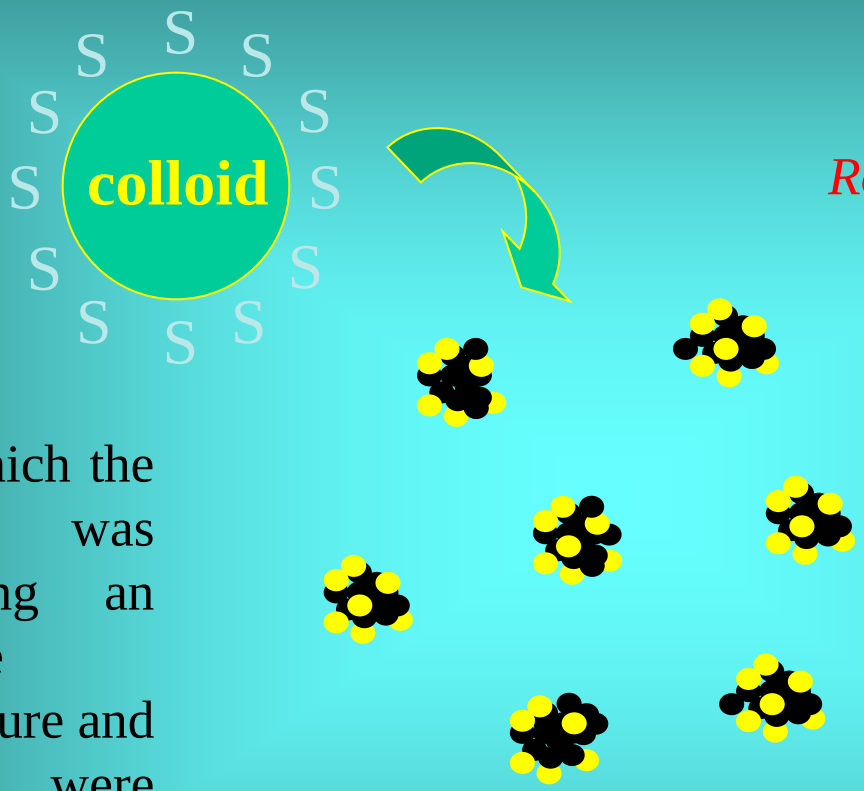

Route D: simple drying

Route E: in which the surfactant was extracted using an ethanol-heptane azeotropic mixture and the catalysts were simple dried

Route C: the dried catalysts were calcined in air at 723 K and then reduced at the same temperature

Route R: thr dried catalysts wre directly reduced in hydrogen at 723 K

Eur. J. Inorg. Chem., (2000) 819-822.

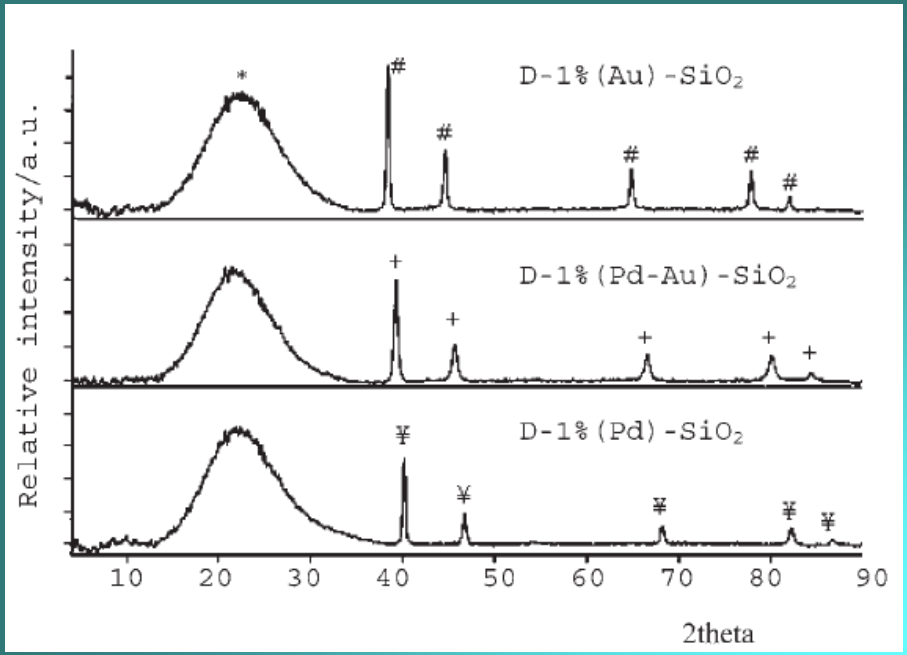

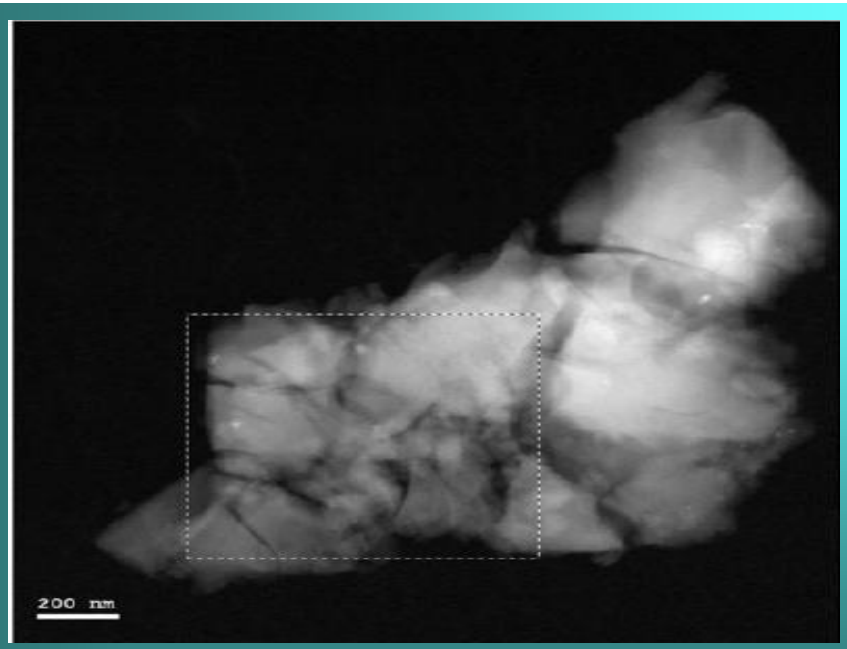

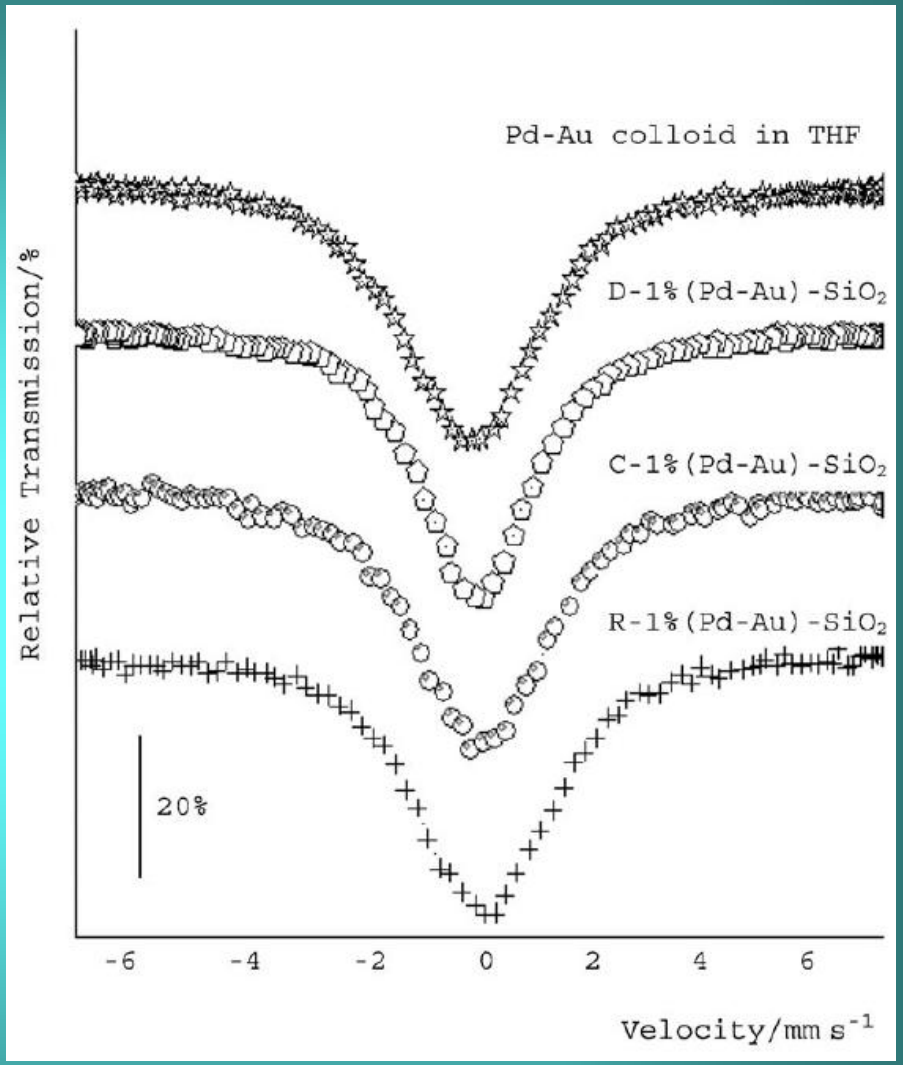

Chem. Eur. J. 2006, 12, 2343 – 2357

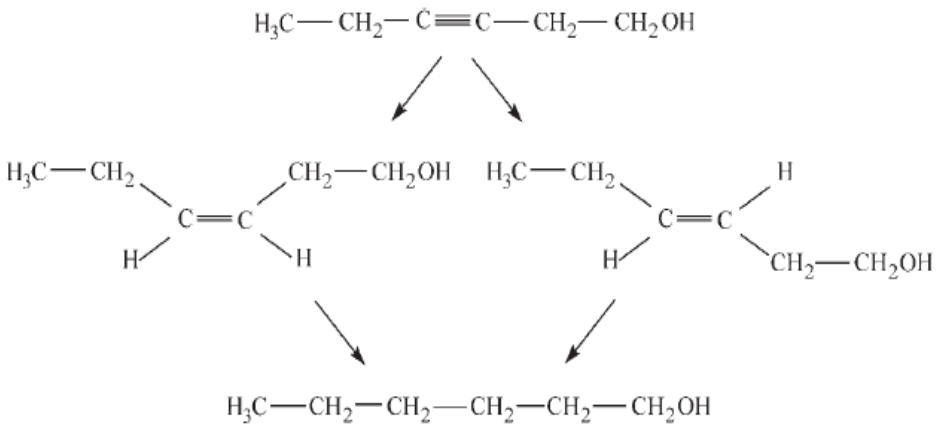

Scheme 3. Hydrogenation of 3-hexyn-1-ol.

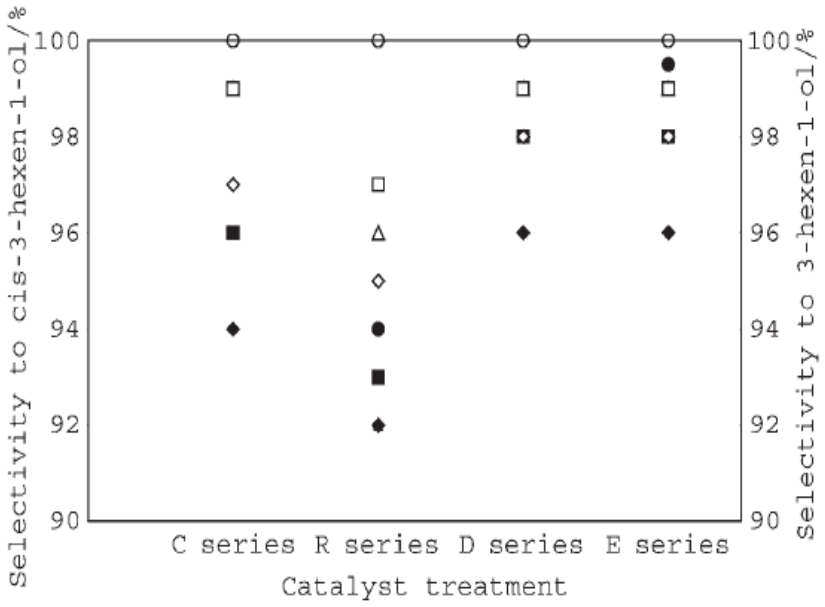

The chemoselectivity to 3-hexen-1-ol(◇,△,○,○) and regioselectivity for cis-3-hexen-1-ol (◆,▲,■,●) on the catalysts differently pretreated (◇,◆ -1%(Pd);△,▲- 0.6%(Pd); □,■- 1%(Pd-Au); ○,●-1%(Au))

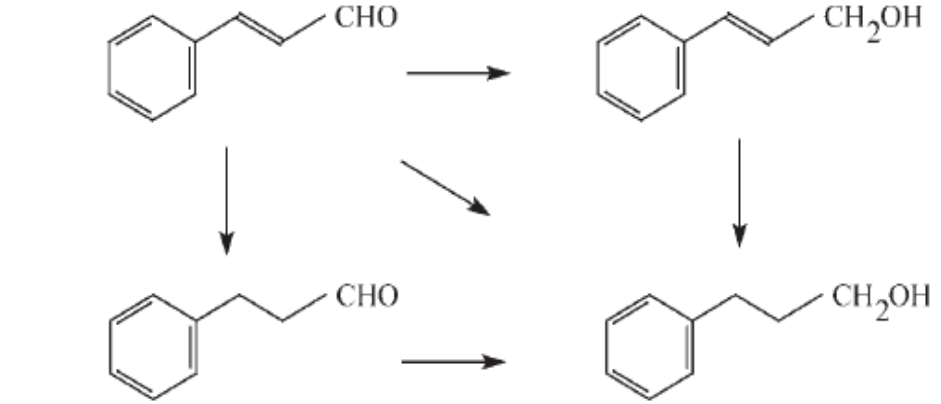

Scheme 4. Hydrogenation of cinnamaldehyde.

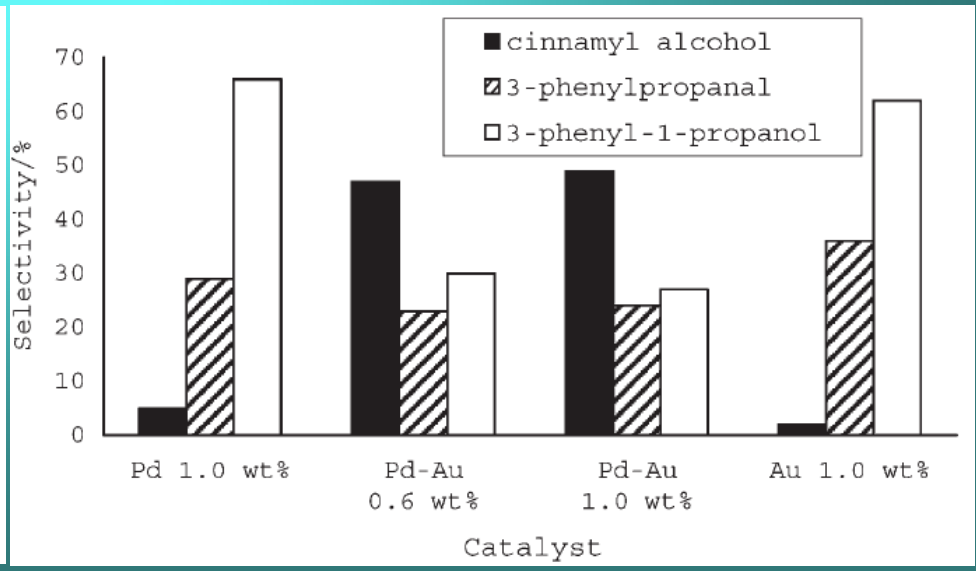

reduction of NO and NO_2 by isopentane under lean conditions

Ligands used in stabilization of the colloids, the amount of recovered Pt and the mean particle size

Colloid	Stabilizing ligands	Chemical formula	Recovered Pt in isolated colloid [%]	Mean particle size [nm]
Pt-1	$N^{+}(C_8H_{17})_4Br$	tetraoctylammonium bromide	83	3
Pt-2	QUAB 342	3-chloro-2-hydroxy-propyl dimethyldodecyl ammonium chloride	81	3
Pt-3	ARQUAD 2HT-75	distearyldimethylammonium chloride	80	3
Pt-4	2-hydroxy-propionic acid	2-hydroxy-propionic acid	58	12.5
Pt-5	REWO PHAT E1027	alkylphenol-polyglycol ether phosphate ester	68	5
Pt-6	TWEEN 40	polyoxyethylene sorbitan monopalmitate	64	7
Pt-7	polyethyleneglycol dodecylether	polyethyleneglycol dodecylether	69	5

Table 2. Textural properties of SiO_2 and SiO_2–Ta_2O_5 embedded Pt colloids after calcination at 773 K.

Colloid	SiO_2 embedded Pt			SiO_2–15 %Ta_2O_5 embedded Pt		
	Pt content [wt %]	Surface area [$m^2 g^{-1}$]	Pore size [nm]	Pt content [wt %]	Surface area [$m^2 g^{-1}$]	Pore size [nm]
Pt-1	2.93	416	3.1	2.95	446	3.1
Pt-2	2.98	423	4.4	2.92	467	4.4
Pt-3	2.97	386	5.4	2.94	432	5.4
Pt-4	3.04	235	2.9	2.98	265	2.9
Pt-5	2.95	326	4.5	2.99	343	4.5
Pt-6	2.96	276	3.5	3.03	298	3.5
Pt-7	2.97	460	4.2	2.93	495	4.1

Table 3. Textural properties of SiO_2 and SiO_2–Ta_2O_5 embedded Pt colloids after extraction with ethanol–heptane azeotropic mixture.

Catalyst	Si–Pt supports			SiTa–Pt supports		
	Pt extracted [wt %]	Surface area [$m^2 g^{-1}$]	Pore size [nm]	Pt extracted [wt %]	Surface area [$m^2 g^{-1}$]	Pore size [nm]
Pt-1	79	523	6.2	81	553	6.4
Pt-2	81	491	13.0	82	501	13.2
Pt-3	83	459	7.2	85	472	7.5
Pt-4	88	645	5.8	91	623	6.2
Pt-5	91	435	9.5	93	432	9.6
Pt-6	90	421	9.0	91	437	9.1
Pt-7	90	659	5.6	92	671	5.8

ChemPhysChem 2007, 8, 666 – 678

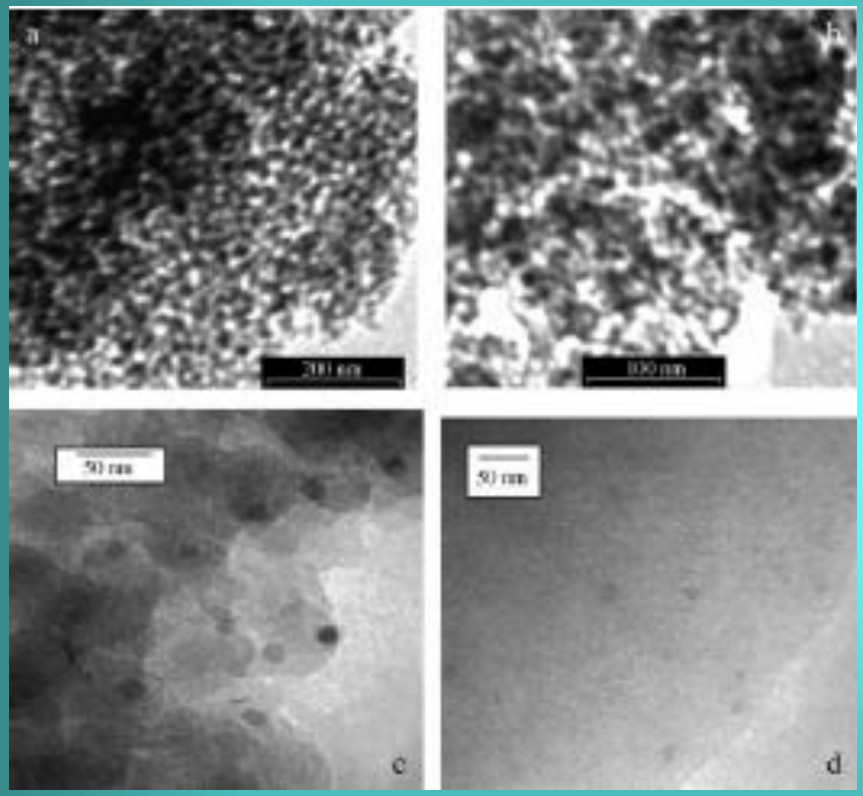

TEM : a) Si–Pt-3; b) Si–Pt-1; c) SiTa–Pt-7; d) Si–Pt-5

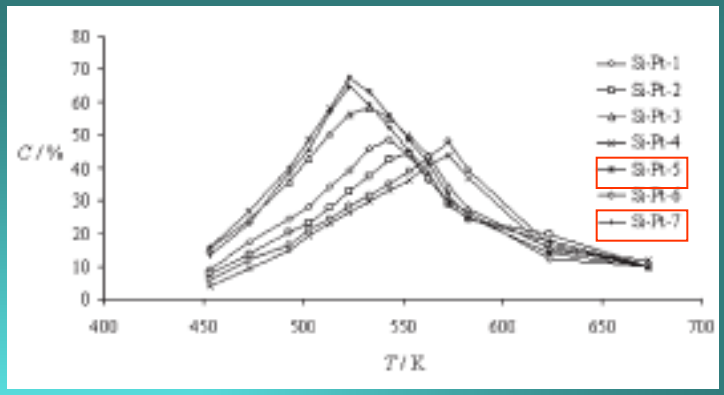

NO conversion on Si–Pt catalysts (5000 ppm NO, 5000 ppm isopentane,and 5% vol. O_2, 100 mg, W/F=2 $gsmL^{-1}$)

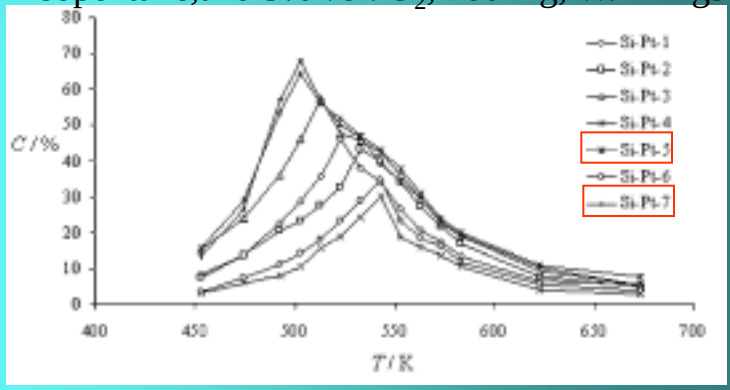

NO_2 conversion on Si–Pt catalysts (5000 ppm NO, 5000 ppm isopentane,and 5% vol. O_2, 100 mg, W/F=2 $gsmL^{-1}$)

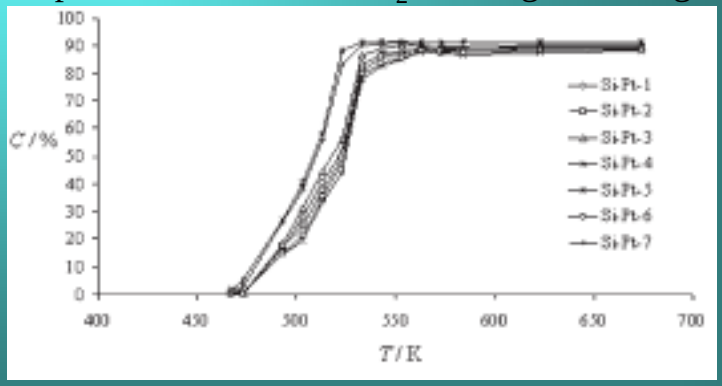

Isopentane conversion on Si–Pt catalysts (5000 ppm NO, 5000 ppm isopentane and 5% vol. O_2, 100 mg, W/F=2 $gsmL^{-1}$)

Size dependent selectivity in deNOx processes

$16\ NO + C_5H_{12} \longrightarrow 8N_2 + 5\ CO_2 + 6\ H_2O$

$96\ NO + 3C_5H_{12} \longrightarrow 48\ N_2O + 15\ CO_2 + 18\ H_2O$

$2NO + O_2 \longrightarrow 2NO_2$

$8NO_2 + C_5H_{12} \longrightarrow 4N_2 + 5\ CO_2 + 6\ H_2O$

$16\ N_2O + C_5H_{12} \longrightarrow 16\ N_2 + 5CO_2 + 6H_2O$

$C_5H_{12} + 8O_2 \longrightarrow 5\ CO_2 + 6\ H_2O$

Table 6. Selectivity of conversion to N_2 and N_2O on the investigated catalysts in reduction of NO at maximum conversion.

Colloid	Si–Pt catalysts			SiTa–Pt catalysts		
	T^a_{max} [K]	N_2 [%]	N_2O [%]	T^a_{max} [K]	N_2 [%]	N_2O [%]
Pt-1	543	53	47	523	51	49
Pt-2	553	51	49	523	52	48
Pt-3	533	55	45	543	48	52
Pt-4	573	38	62	573	36	64
Pt-5	523	65	35	553	44	56
Pt-6	573	42	58	573	38	62
Pt-7	523	64	36	553	43	57

Table 7. Selectivity of conversion to N_2 and N_2O on the investigated catalysts in reduction of NO_2.

Colloid	Si–Pt catalysts			SiTa–Pt catalysts		
	T^a_{max} [K]	N_2 [%]	N_2O [%]	T^a_{max} [K]	N_2 [%]	N_2O [%]
Pt-1	523	65	35	503	68	32
Pt-2	533	62	38	503	69	31
Pt-3	513	70	30	523	61	39
Pt-4	543	48	52	533	42	58
Pt-5	503	74	26	523	58	42
Pt-6	543	53	47	543	44	56
Pt-7	503	72	28	533	55	45

The selectivity for conversion to N_2 reached 74% for Si–Pt-5, which may suggest that indeed a mean particle size between 8 and 10 nm is the most effective for this reaction.

ChemPhysChem 2007, 8, 666 – 678

Un-expected selectivity

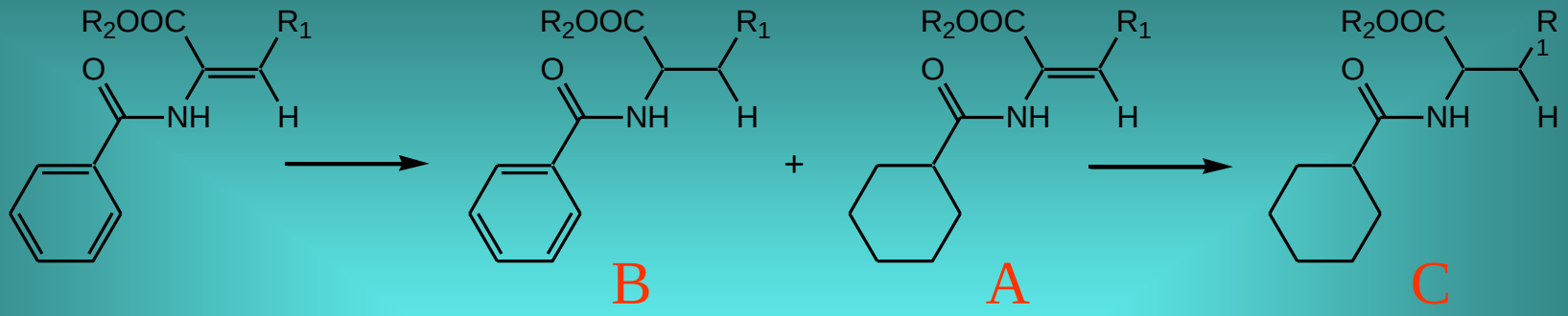

R_1:

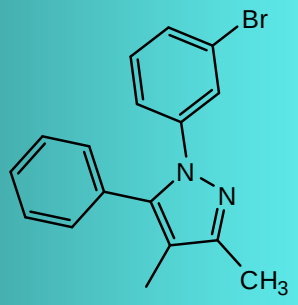

V1

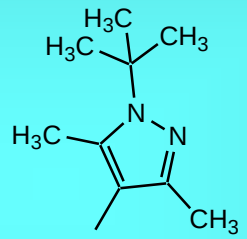

V2

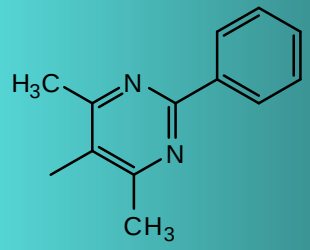

V3

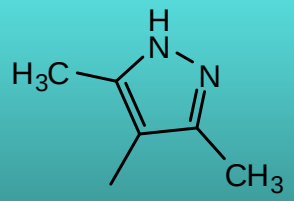

V4

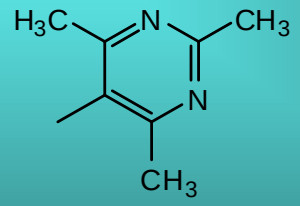

V5

Angew. Chem. Int. Ed., 48 (2009) 1085 –1088.

The CO_2-induced melting point depression during the reduction step allows the use of simple ammonium salts that would not classify as ionic liquids, resulting in solid and easy to handle catalyst materials.

Generation of matrix-embedded rhodium nanoparticles by reduction in CO_2-induced ionic liquids. - *Left:* Physical mixture of ammonium salt and solid organometallic precursor; *Middle*: Reduction under CO_2/H_2 in the CO_2 induced ionic liquid phase (view into the high pressure reactor including the magnetic stir bar); *Right*: Solid material containing the embedded nanoparticles obtained after venting the reactor.

Angew. Chem. Int. Ed., 48 (2009) 1085 –1088.

Selected characteristic data for rhodium nanoparticles embedded in solid ammonium salts that were generated by CO_2-induced ionic liquid phases[a]

Catalyst	Matrix	M.p. [^{0}C]	T [^{0}C]	p[b] [bar]	Particle size [nm]	Surface to bulk atom ratio	Rh(0) to Rh(I) ratio from XPS
Rh-1	$[Bu_4N]Br$	124[c]	80	240	3.3 1.5	0.33	0.63
Rh-2	$[Hex_4N]Br$	100[c]	40	150	2.3 ±0.8	0.47	0.62
Rh-3	$[Oct_4N]Br$	98[c]	60	220	1.4 ±0.3	0.78	0.59

[a] Reaction conditions: ionic matrix (0.5 g), precursor [Rh(acac)(CO)2] (1% Rh), H2 (40 bar), and scCO2 (density: ca. 0.7 gmL1), 180 min. [b] Total pressure at reduction temperature. [c] Melting points of the pure matrix under standard conditions.

Angew. Chem. Int. Ed., 48 (2009) 1085 –1088.

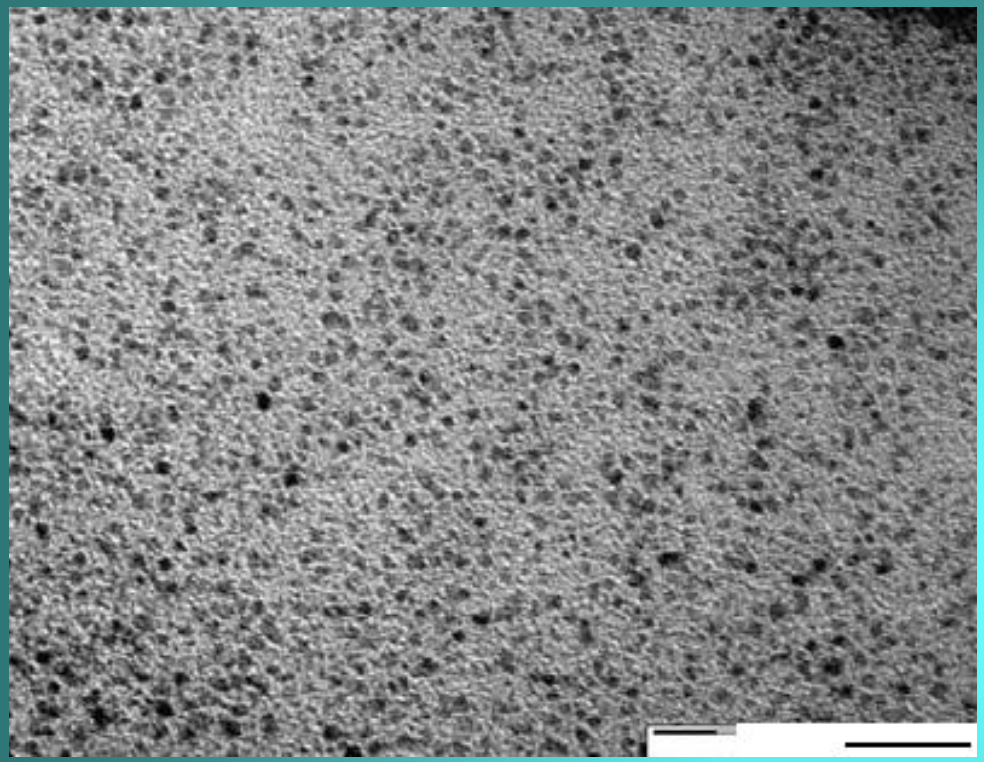

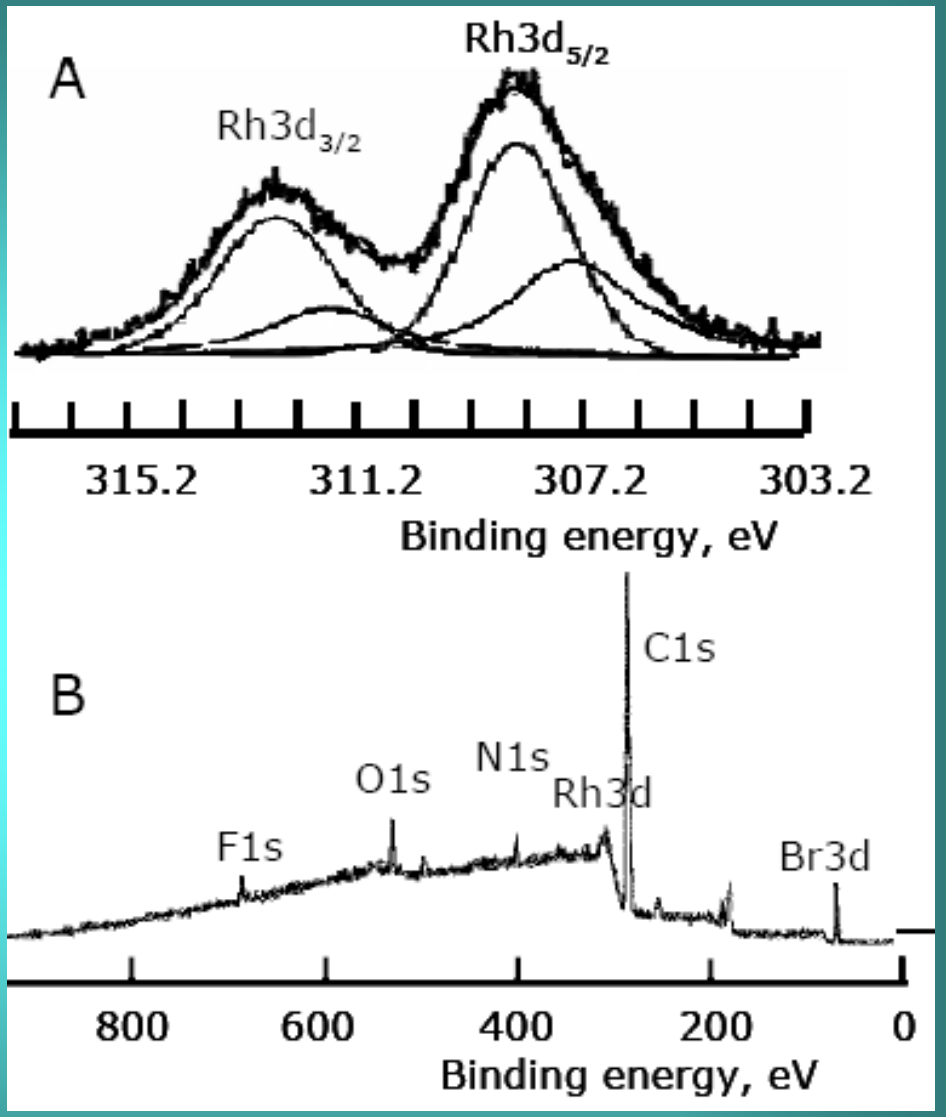

Representative TEM micrograph (left, bar = 20 nm) and XPS spectra (right; A: expansion of the rhodium signals) of rhodium nanoparticles generated from [(acac)Rh(CO)$_2$] in [Hex$_4$N]Br (**Rh-2**); B: overview;

Representative catalytic results for benchmark reactions using matrix-embedded rhodium nanoparticles.[a]

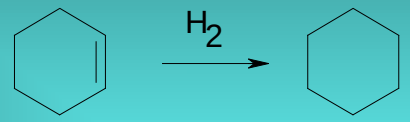

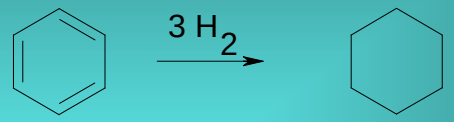

Catalyst	Phase behavior	TOF_{total}[b] [h^{-1}]	$TOF_{surface}$[c] [h-1]	Phase behavior	TOF_{total}[b] [h^{-1}]	$TOF_{surface}$[c] [h^{-1}]
Rh-1	immiscible	8800	26650	partially miscible	35	106
Rh-2	partially miscible	6600	14050	partially miscible	8	17
Rh-3	partially miscible	35700	45800	partially miscible	42	54

[a] Reaction conditions: T=408C, p(H2)=40 bar, neat; 1: Rh=1000:1, 2: Rh=100:1. [b] Total turnover frequency determined as mol substrate per total amount of rhodium in matrix per hour, determined from hydrogen uptake within the first 20% conversion; full conversion was reached in all cases after appropriate reaction time. [c] Turnover frequency corrected for surface-exposed rhodium centers by using the dispersion data

Selective hydrogenation of (E)-2-(benzoylamino)-2-propenoic acids using Rh-1 as catalyst

V-R2 Substrates	Reaction conditions			TOF[b] x 10^3, min^{-1}	Selectivity[a], %			
	T, ^oC	Pres. H_2, barr	CO_2, g		A	B	C	C’
V1-H	120	100	-	114.6	39	24	37	-
V1-H	120	100	7.5	11.7	49	21	30	-
V2-H	80	100	-	2614.3	30	54	16	-
V2-H	80	100	7.5	319.3	46	32	22	-
V3-Me	60	100	-	96.3	13	18	60	9
V3-Me	60	100	7.5	51.9	39	31	25	5
V3-H	60	100	-	79.6	6	56	38	-
V3-H	60	100	7.5	41.1	17	51	32	-
V4-H	60	100	-	267.5	4	96	-	-
V4-H	60	100	7.5	122.4	100	-	-	-
V5-H	80	100	-	15.9	100	-	-	-

Ionic nanostructures

Angew. Chem. Int. Ed., doi: 10.1002/ANIE.201002090

Thus, the Au environment found for the sample Au-100 (3.6 Cl at 2.281 Å) closely resembles that in the tetrachloroauric acid structure, consisting of 6 Cl atoms at 2.286 Å. This points out the precursor preservation after the thermal treatment at 100°C. The reduced number of Cl neighbours in the structure of the sample Au-100 could indicate a Cl-defective structure of the precursor, but also small precursor particles, influencing a lowering of the coordination number derived by EXAFS. By increasing the treatment temperature to 150°C, a large fraction of gold reduces to metallic state.

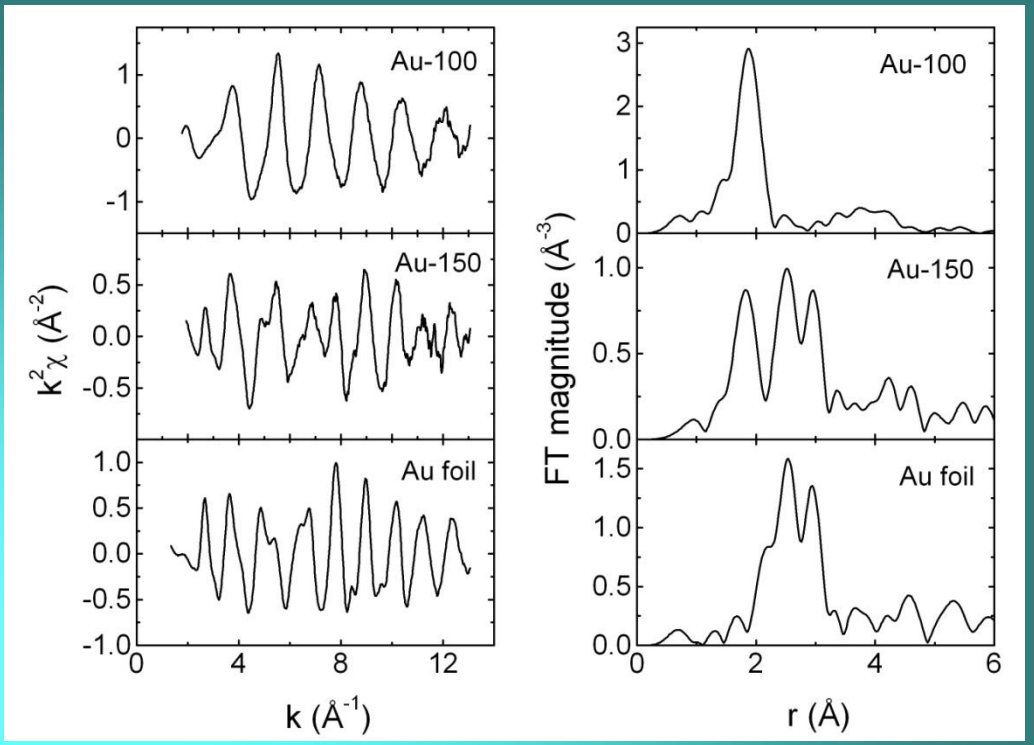

k^2-weighted EXAFS spectra of the Au catalysts and Au foil and magnitude of the corresponding Fourier transforms.

Au environment in the investigated Au catalysts, as inferred by the fit of EXAFS.

Sample	*CN*	*R* (Å)	σ^2 (10^{-3} Å^2)	Filtered *r*-range (Å)	R-factor
Au-100	3.6 0.6 Cl	2.281 0.006	2 1	1.4–2.3	0.056
Au-150	1.3 0.3 Cl	2.26 0.01	3 2	1.3–3.3	0.124
	6 1 Au	2.883 0.005	6 1		
Au foil	12 Au	2.884		1.8–3.3	

Comparison of the gold based catalysts in terms of conversion (X) and overall selectivity (S) and diastereoselectivity (ds)[a]

Sample	X (%)	Overall $S_{isopulegols}$ (%)	$S_{menthols}$ (%)
MgF_2[b]	95.0	87.0	-
Au-100	99.0	57.0	43.0
Au-150	0.5	0	0
Au-100[c]	99.0	39.2	60.8
Au-100[d]	99.0	7.5	92.5

[a] Reaction conditions: 100 mg catalyst, 1.0 mL (860 mg) citronelal, 5 mL toluen, 80° C, 15 atm H_2, 22h; [b] –the cyclisation of citronellal to isopulegol: 100 mg catalyst, 1.0 mL citronelal, 5 mL toluene, 80° C, 6h; [c]- the second catalytic charge; [d]- the third catalytic charge

Catalytic pathway

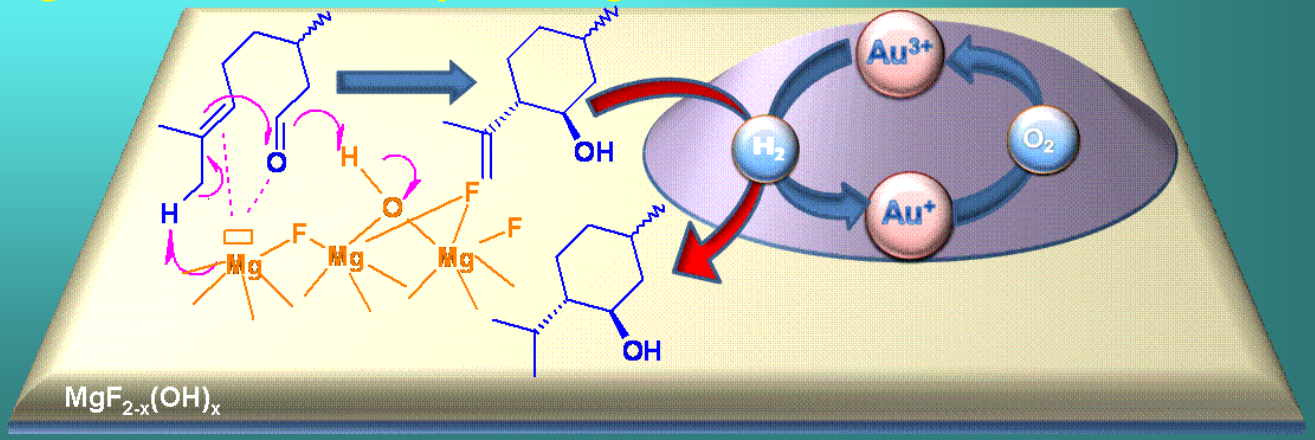

Angew. Chem. Int. Ed., doi: 10.1002/ANIE.201002090

Size Tunable Gold Nanorods Evenly Distributed in the Channels of Mesoporous Silica

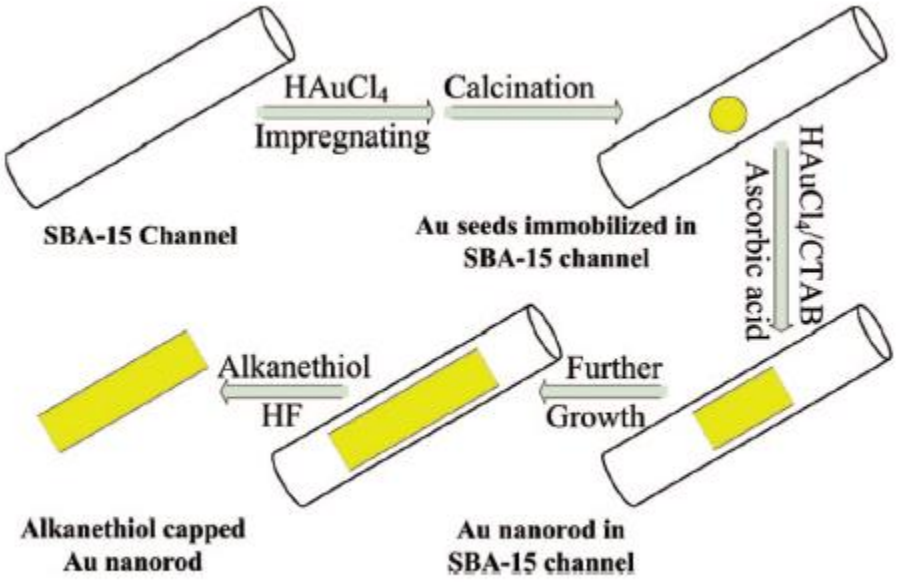

Scheme 1. Synthesis scheme of *in situ* growth of gold nanorods in the channels of SBA-15.

TABLE 2. N_2-Adsorbption Data and Length of Nanorods in Different Samples

	S_{BET} (m^2/g)[a]	V_{BJH} (cc/g)[b]	D_{BJH} (nm)[b]	length of rods (nm)[c]
SBA-15	613	0.899	4.89	
APTES-SBA-15	436	0.721	4.88	
seeds/SBA-15	421	0.697	4.93	3—5 (spheres)
rods40/SBA-15	400	0.662	4.88	20—30
rods100/SBA-15	372	0.691	4.83	30—50
rods400/SBA-15	410	0.654	5.53	100—200

[a]The surface area S_{BET} is calculated by BET method. [b]The pore volume and the pore size distribution are determined by the BJH model applied to the desorption branch of isotherm. [c]The length of nanorods is determined by TEM.

ACS Nano, 2 (2008) 1205–1212

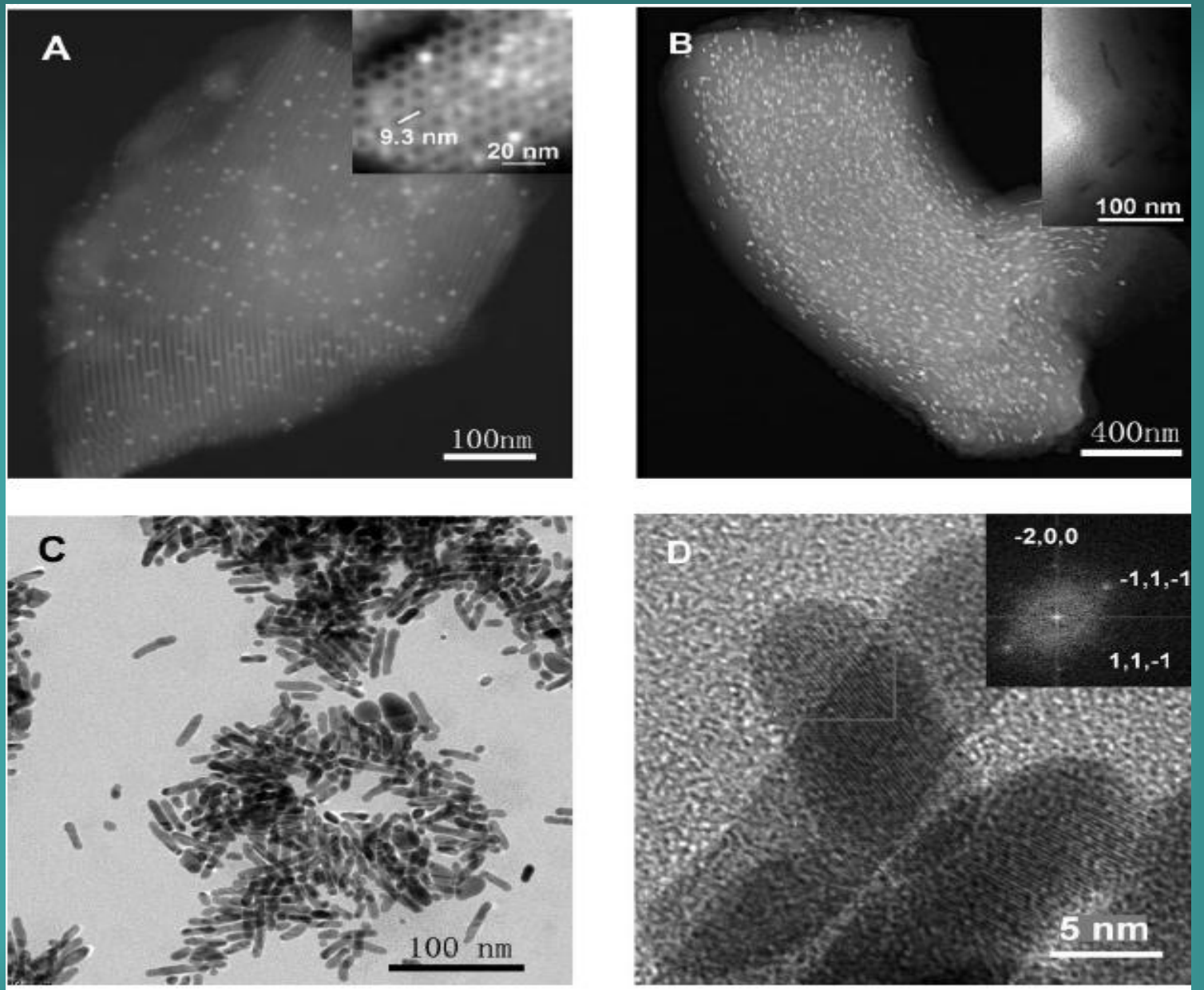

Figure 1. HAADF-STEM images of the (A) seeds/SBA-15 and (B) rods100/SBA-15 (inset is a BF-TEM image at higher magnification); (C) BF-TEM image of unsupported Au rods after removing silica matrix; and (D) HR-TEM image of single-crystalline domain at unsupported Au rods (the inset shows the corresponding fast Fourier transform of the area indicated).

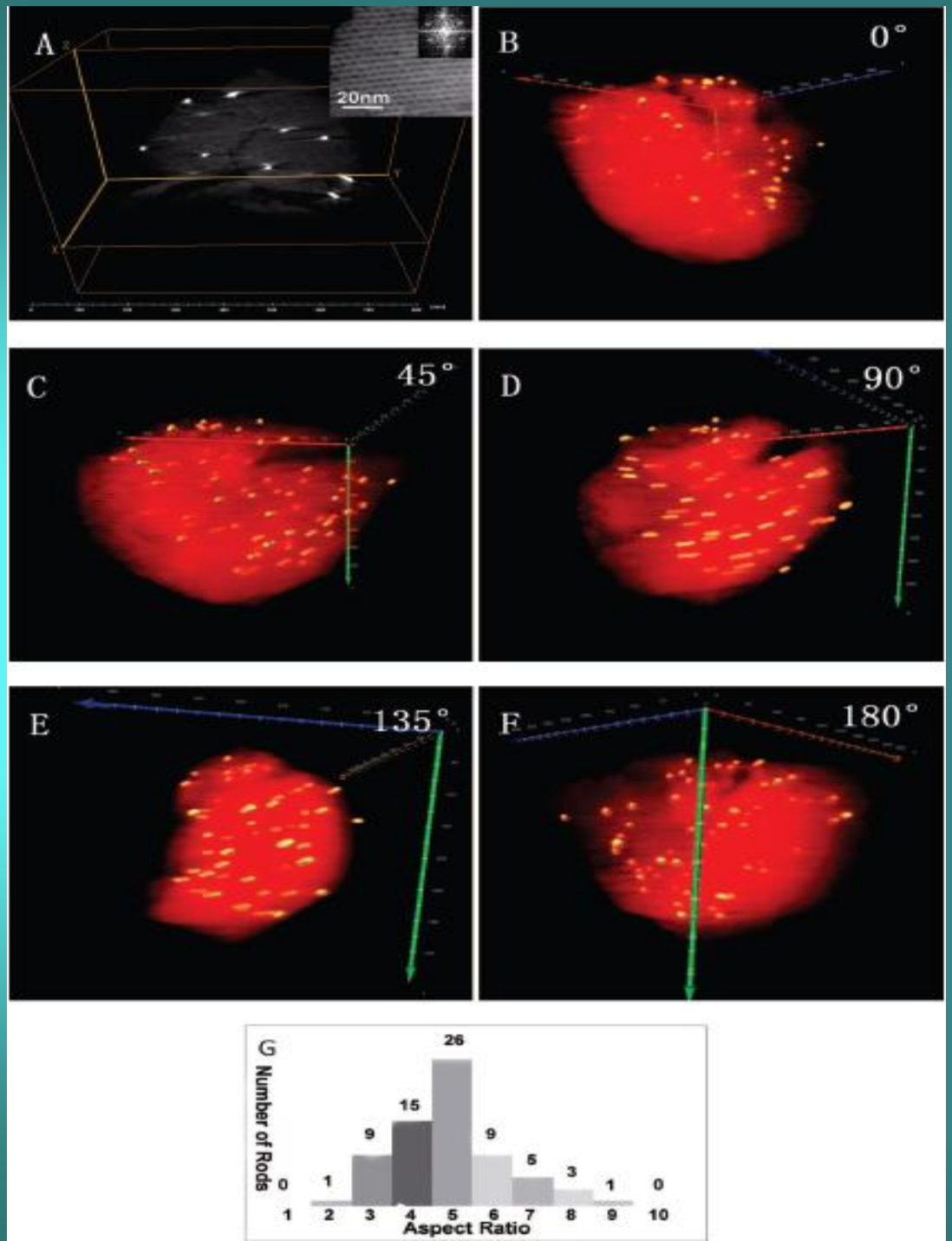

Figure 2. Tomography visualization of rods100/SBA-15: (A) digital slices though the reconstructed volume (the inset is the fast Fourier transform of order porous structure of SBA-15); (BF) overall visualization of the gold nanorods embedded in a small piece of SBA-15 viewed from diffrent directions; and (G) the aspect ratio statistics of the rods.

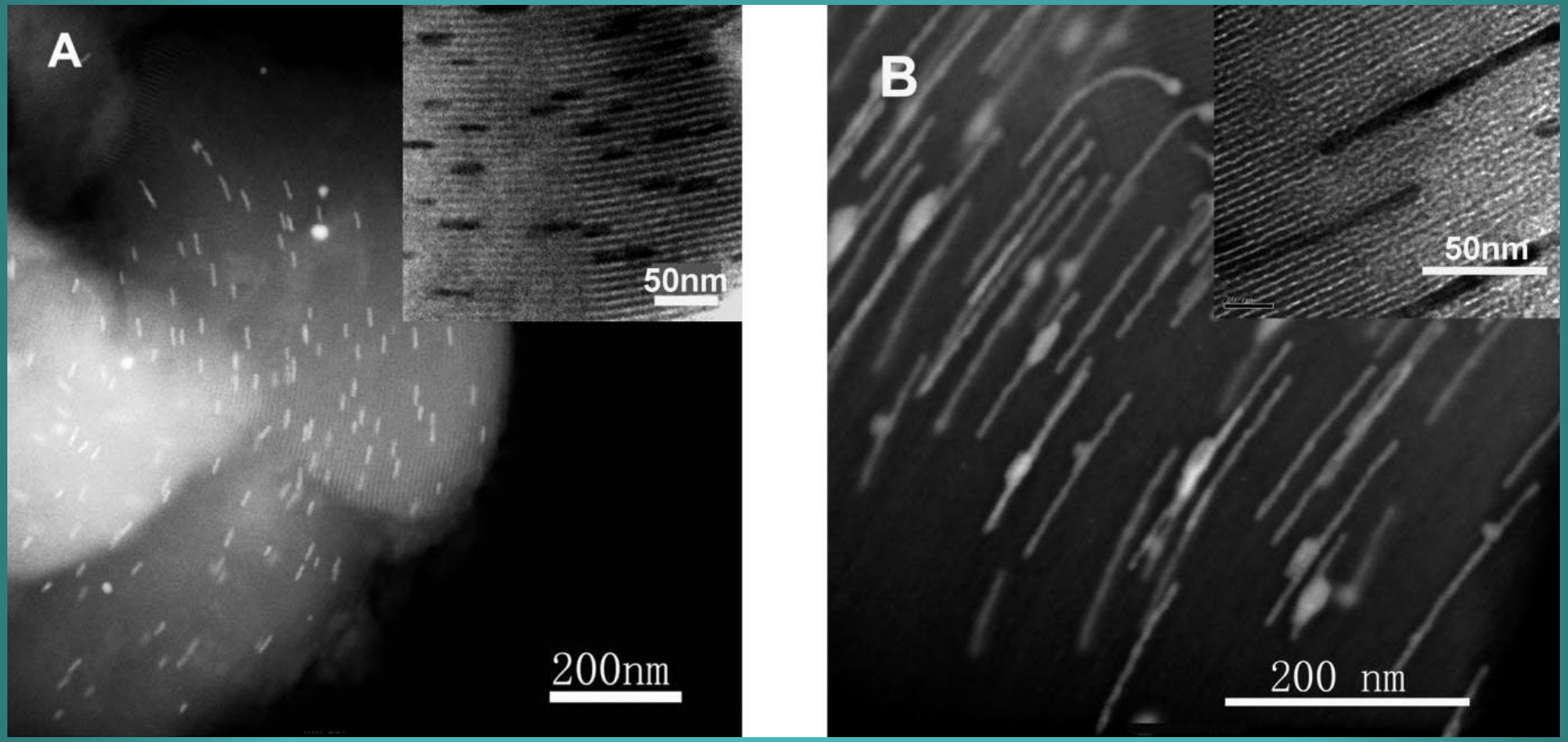

Figure 3. HAADF-STEM images of the (A) rods40/SBA-15 and (B) rods400/SBA-15. The insets are the BF-TEM images at higher magnification

Acknowledgements

Professors:

Christopher Hardacre

Ryan Richards

Walter Leitner

Simona M. Coman

Jean-Pierre Genêt

Véronique Michelet

Hans-Peter Steinrück

J. Michael Gottfried

A.v. Humboldt Foundation

PhD

Florentina Neațu

PhD

Valentin Cimpeanu

PhDs:

Cristina Paun

Roxana Bota

PNCDI II, parteneriate
Cooperari
interguvernamentale

Catalytic reaction

Cram rule

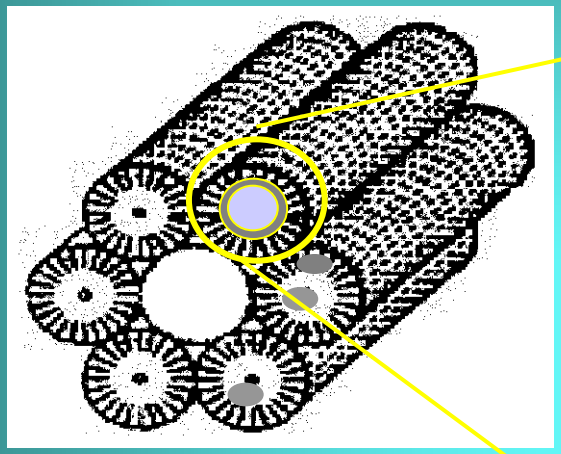

MCM-41, S_{sp}=1083 m^2/g

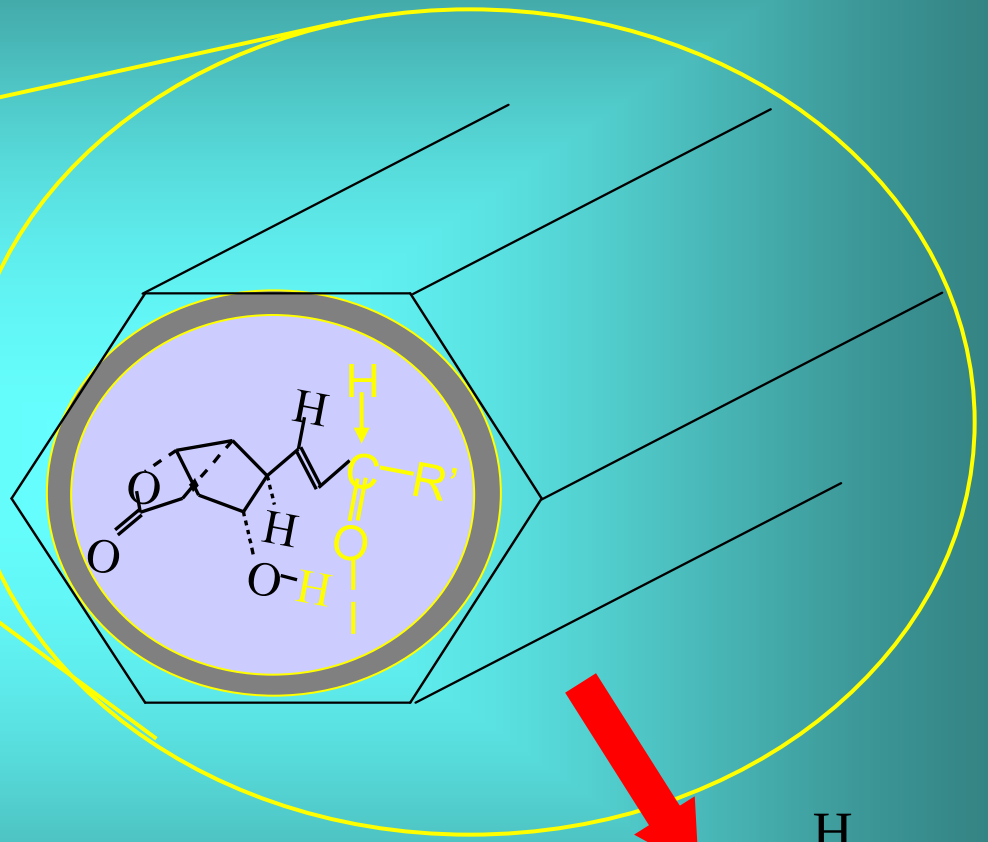

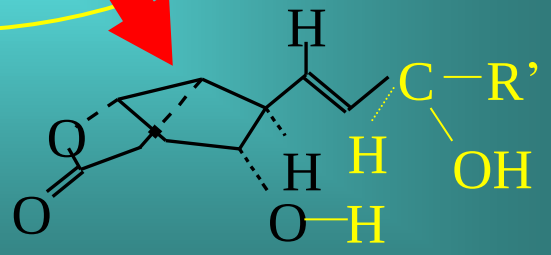

Endo control of the selectivity